Plant, Cell and Environment (2007) **30**, 600–616 doi: 10.1111/j.1365-3040.2007.01647.x

Variations in ^{13}C discrimination during CO_2 exchange by *Picea sitchensis* branches in the field

LISA WINGATE[1,2]*, ULLI SEIBT[3,4,5]*, JOHN B. MONCRIEFF[1], PAUL G. JARVIS[1] & JON LLOYD[3,6]

[1]School of GeoSciences, University of Edinburgh, Edinburgh, UK, EH9 3JU, [2]INRA-EPHYSE, 33833 Villenave d'Ornon Cedex, France, [3]Max Planck Institute for Biogeochemistry, Jena, Germany, [4]Department of Global Ecology, Carnegie Institution of Washington, Stanford, CA, USA, [5]Department of Plant Sciences, University of Cambridge, Cambridge, UK and [6]School of Geography, University of Leeds, Leeds, UK

ABSTRACT

We report diurnal variations in ^{13}C discrimination ($^{13}\Delta$) of *Picea sitchensis* (Bong.) Carr. branches measured in the field using a branch chamber technique. The observations were compared to predicted $^{13}\Delta$ based on concurrent measurements of branch gas exchange. Observed $^{13}\Delta$ values were described well by the classical model of $^{13}\Delta$ including isotope effects during photorespiration, day respiration and CO_2 transfer through a series of resistances to the sites of carboxylation. A simplified linear of model $^{13}\Delta$ did not capture the observed diurnal variability. At dawn and dusk, we measured very high $^{13}\Delta$ values that were not predicted by either of the said models. Exploring the sensitivity of $^{13}\Delta$ to possible respiratory isotope effects, we conclude that isotopic disequilibria between the gross fluxes of photosynthesis and day respiration can explain the high observed $^{13}\Delta$ values during net photosynthetic gas exchange. Based on the classical model, a revised formulation incorporating an isotopically distinct substrate for day respiration was able to account well for the high observed dawn and dusk $^{13}\Delta$ values.

Key-words: branch chambers; carbon isotopes; day respiration; photosynthetic discrimination.

INTRODUCTION

Nearly 30% of the entire atmospheric pool of CO_2 (750 Gt) is exchanged across leaf surfaces each year. The $\delta^{13}C$ enrichment that accompanies the summer drawdown of CO_2 in the atmosphere can be ascribed to photosynthetic discrimination against $^{13}CO_2$ by the terrestrial biosphere. Globally, photosynthetic uptake of CO_2 discriminates by 15 to 18‰ against ^{13}C (weighted mean of C_3 and C_4 vegetation, Lloyd & Farquhar 1994). For plants with the C_3 photosynthetic pathway, the photosynthetic discrimination against ^{13}C ($^{13}\Delta$) has been related to the lower reactivity of ^{13}C during fixation by photosynthetic enzymes, as well as to differential diffusivities of $^{13}CO_2$ and $^{12}CO_2$ in air (Farquhar, O'Leary & Berry 1982; O'Leary 1984). The magnitude of photosynthetic ^{13}C discrimination is sensitive to environmental variables such as vapour pressure deficit, photon flux density and air temperature. The $\delta^{13}C$ composition of CO_2 thus provides a natural tracer for component processes and their regulation by environmental conditions.

The $\delta^{13}C$ signature of photosynthetic fluxes often responds differently to changes in environmental conditions than that of concurrent plant and soil respiratory fluxes, creating transient isotopic disequilibria (Lloyd *et al.* 1996). This is employed at the ecosystem and global scales to interpret field data and to simulate isotopic gas exchange between the terrestrial biosphere and the atmosphere with numerical models. For example, time series of the $\delta^{13}C$ of atmospheric CO_2 are tools in inversion studies for tracking changes in CO_2 fluxes of the terrestrial biosphere and ocean in response to climate variability (Tans, Berry & Keeling 1993; Francey *et al.* 1995). Plant physiology models incorporating carbon isotope ratios are important for predicting the influence of different biomes on the global patterns of $\delta^{13}C$ in atmospheric CO_2, providing a tool for constraining large-scale fluxes (Lloyd & Farquhar 1994; Randerson *et al.* 2002). At the ecosystem scale, partitioning may be possible at sites measuring eddy flux and CO_2 concentration profiles with observations of the $\delta^{13}C$ composition of CO_2 (Lloyd *et al.* 1996; Yakir & Wang 1996; Bowling, Tans & Monson 2001; Ogée *et al.* 2003, 2004).

But field measurements of photosynthetic ^{13}C discrimination have only been reported for a few ecosystems (Harwood 1997; Harwood *et al.* 1998). Thus, a gap exists between studies of photosynthetic ^{13}C discrimination at the leaf scale (generally conducted under steady-state conditions in the laboratory) on the one hand, and the interpretation of field data and modelling at the ecosystem and global scale on the other. We try to link these scales by exploring the natural variability of ^{13}C discrimination at the largest scale possible for direct measurements: whole branches enclosed in chambers. Through this choice of scale and method of observation, we have a useful platform for making observations under field conditions relevant for the

Correspondence: L. Wingate Fax: +44 (0) 131 662 0478; e-mail: l.wingate@ed.ac.uk

*These authors contributed equally to the work.

interpretation of isotopic data at increasing temporal resolution (Bowling *et al*. 2003, 2005; Griffis *et al*. 2004; Griffis, Baker & Zhang 2005).

Here, we present daily variations in environmental conditions, CO_2 and water fluxes of branches in a *Picea sitchensis* (Bong.) Carr. plantation in central Scotland alongside concurrent measurements of discrimination against ^{13}C ($^{13}\Delta_{obs}$) in the field. This paper demonstrates how trace gas measurements during 5 min closure intervals of branch chambers can be used to: (1) obtain diurnal data sets of $^{13}\Delta_{obs}$ from flask observations in the field; (2) derive estimates of ^{13}C discrimination from gas-exchange and microclimate data that are directly comparable to the flask observations; and (3) derive $^{13}\Delta$ estimates that correspond to those expected in the absence of chambers. We also explore the sensitivity of net ^{13}C discrimination to isotope effects during internal CO_2 transfer, photorespiration and day respiration.

MATERIALS AND METHODS

Study site and gas-exchange measurements

The study was made in Griffin Forest, an even-aged plantation of Queen Charlotte Islands provenance *P sitchensis* (Bong.) Carr. located near Aberfeldy, Perthshire, UK (56°37′N, 3°48′W). A description of the site, a long-term monitoring station within the CARBOEUROPE-IP network can be found at http://www.carboeurope.org.

Three branch chambers constructed from extruded acrylic and polypropylene film (34 μm thick, ICI Propafilm, Dumfries, UK) were installed on two trees of 13.6 and 9.5 m height within a 0.01 ha plot from 18 May 2001 to 22 July 2001. Bud burst was partially occurring in the canopy in May, while in July shoot expansion was complete. Branches were chosen as representative of sun-lit branches visible from the tower. Two branches were used in the upper canopy at 10.5 m (chamber 1) and 9.4 m (chamber 3) and one in the middle canopy at 8.1 m (chamber 4) in height. During the July campaign, chamber 4 was sealed without a branch inside and designated as a control. Chambers were positioned to the south of the tower to minimize shading effects. They were held in position by metal booms projecting from the canopy access tower and nylon cord, allowing the chambers to move with the branches. The chambers are fully described by Rayment & Jarvis (1999) and Wingate (2003). The experimental set-up has been used to investigate branch O_2:CO_2 exchange and ^{18}O discrimination (Seibt *et al*. 2004, 2006). The latter also employed the same simulation approach as the present study.

During the day, the bags were closed for 5 min, after which they were opened and ventilated for 15 min, i.e. measurements were made on each branch every 20 min. At night, they were closed for 10 min and ventilated for 30 min, i.e. the measurement cycle changed to every 40 min. During closure periods, relative humidity (h) and air temperature (T_a) were monitored within each bag [Vaisala HMP 35A; Vaisala (UK) Ltd, Cambridge, UK]. Needle temperature (T_l) was measured in three locations per chamber (0.2 mm in diameter Cu-Con thermo-junction, referenced to air temperature). Photosynthetic photon flux density (Q) incident upon each branch was measured using a photosynthetic photon flux density sensor (SD101QV; Macam Ltd, Livingston, UK) attached vertically on the branch midway along its length. At the same time, the CO_2 mole fraction of chamber air was monitored with an infrared gas analyser (IRGA) (LI-6262; Li-Cor Inc., Lincoln, NE, USA). Outputs were recorded with a logger (CR10; Campbell Scientific Ltd, Shepshed, UK) that also served to initiate the measurement sequence. The CO_2 concentration in reference bottles of air was calibrated against gas mixtures prepared by mixing pure CO_2 with CO_2-free air using three precision gas mixing pumps (G27/3F, SA18/3F and SA17/3F; H.Wösthoff GmbH, Bochum, Germany). H_2O vapour span was set using a dew point generator (LI-610; Li-Cor Inc.). The chambers were kept open in a continuously ventilated state when not in use.

Rates of net CO_2 assimilation (A, μmol m^{-2} s^{-1}), transpiration (E, mol m^{-2} s^{-1}) and branch conductances to water vapour and CO_2 (g_s, g_c, mol m^{-2} s^{-1}) were calculated and integrated over the full chamber closure periods (see Appendix I). To calculate the leaf surface CO_2 mole fraction (C_s), the leaf boundary layer conductance for CO_2 inside the chamber (g_b) was estimated as 1.5 ± 0.5 mol m^{-2} s^{-1} from energy balance considerations. The intercellular CO_2 mole fraction incorporating ternary effects (Jarman 1974), $C_{i,g}$ (μmol mol^{-1}), was calculated following the notation of von Caemmerer & Farquhar (1981) as

$$C_{i,g} = \frac{\left(g_c - \frac{E}{2}\right)C_s - A}{\left(g_c + \frac{E}{2}\right)} \quad (1)$$

The subscript g denotes that for a heterogeneous system such an estimate is weighted according to the conductances and not that of A (Farquhar 1989) (see Appendix III).

Collection and analysis of organic material

During the May field campaign, needle and non-green twig samples were collected from the same or adjacent Sitka spruce trees. Samples were taken at the same heights and close to the chamber locations. All samples were stored in glass sample vials, transferred to the laboratory as rapidly as possible and stored at –20 °C until analysis. Samples were dried and ground with a ball mill to a fine homogeneous powder. Subsamples were weighed and their carbon isotope ratios determined on an elemental analyser (NA 1110 CN; CE Instruments, Rodano, Italy), coupled via open split interface to a mass spectrometer (ConFlo III and Delta$^+$XL; both Finnigan MAT, Bremen, Germany). SD for dry matter $\delta^{13}C$ was 0.05‰. The samples were analysed at the Max Planck Institute for Biogeochemistry, Jena, Germany.

Collection and analysis of flask samples

Pairs of air samples from branch chambers were collected at intervals of approximately 3 h over 24 h in spring (18/19 May) and summer (20 July) of 2001. Air was circulated from the branch chambers through sampling lines into a flask sampling system (separate from that used for gas-exchange measurements), and back into the chamber. Within the sampling system, the air stream was passed through a magnesium perchlorate cylinder to remove water vapour, and pumped through two flasks in series. We used 1 dm^3 glass flasks with a valve (Glass Expansion, Melbourne, Australia) on each end, sealed with Teflon perfluoroalkoxy (PFA) O-rings (DuPont Fluoro products, Wilmington, DE, USA), and 1.3 dm^3 flasks with two valves (Louwers, Hapert, the Netherlands) on the same end. Flask samples were taken at two points in the sequence of opening and closing of branch chambers. The first flask was collected 3 to 4 min before closure ('open sample') and reflects the CO_2 mole fraction and isotopic signature of ambient canopy air. The second flask ('closed sample') was collected shortly before reopening of the chamber.

The CO_2 mole fractions in the air samples were determined using a gas chromatograph (HP 6890; Hewlett Packard, Palo Alto, CA, USA) linked to a methanizer and flame ionization detector. Subsamples of CO_2 were then extracted cryogenically from the dry air samples ('BGC-AirTrap', Werner, Rothe & Brand 2001), and their isotope ratio determined on a dual inlet isotope ratio mass spectrometer (Delta$^+$XL; Finnigan MAT). The analytical precision was in the order of 0.08 μmol mol^{-1} for CO_2 mole fraction and 0.01‰ for $\delta^{13}C$, reported with respect to V-PDB-CO_2. Uncertainties of flask data were estimated from the SDs of laboratory analysis of duplicate flasks, 0.13 μmol mol^{-1} for CO_2 mole fraction and 0.01‰ for $\delta^{13}C$. Additional uncertainties arising from the sampling procedure, applying to samples collected at the end of closure periods, were estimated from control measurements in an empty chamber. They were 1.3 μmol mol^{-1} for CO_2 mole fraction and 0.2‰ for $\delta^{13}C$.

Calculations of $\delta^{13}C$ signatures of CO_2 exchange from flask data

The observed values of ^{13}C discrimination during photosynthesis, $^{13}\Delta_{obs}$ (‰) of foliage in the closed branch chamber were determined following Guy *et al*. (1989):

$$^{13}\Delta_{obs} = \frac{\ln\frac{\Re_e}{\Re_o}}{\ln\frac{C_e}{C_o}}\left(1+\frac{\ln\frac{\Re_e}{\Re_o}}{\ln\frac{C_e}{C_o}}\right)^{-1}, \qquad (2)$$

where C_o and C_e are the mole fractions (μmol mol^{-1}) and $\Re_o$ and $\Re_e$ the $^{13}C/^{12}C$ ratios of CO_2 at the beginning and end of closure periods, respectively. These correspond to the samples collected from the open and closed chambers for flask measurements, and to starting time values and those integrated over the closure periods for gas-exchange data (see Appendix I). We use Eqn 2 for both flask observations and $^{13}\Delta$ predictions from gas-exchange data (although not strictly valid as $^{13}\Delta$ is changing during the closure period) because it allows us to directly compare the two approaches. Estimated uncertainties for $^{13}\Delta_{obs}$ were calculated using Gaussian error propagation. They were inversely related to net flux rates, usually < 1‰, but > 5‰ at dawn and dusk. Discrimination values were also largest at these times.

All calculations were performed in interactive data language (IDL) (Version 6.1; Research Systems Inc., Boulder, CO, USA). Correlation parameters between predicted and observed $^{13}\Delta$ were obtained from least absolute deviation regressions using the flask observations as independent variable. Four data points were excluded due to lack of reliable gas-exchange measurements (18 May, 0710 h IRGA tubing detached, 0740 h relative humidity constant at 50%, 1740 h sensor artefacts from direct sunlight, 20 July, 0340 h air saturated).

SIMULATIONS

Predictions of $^{13}\Delta$ during foliage gas exchange

We calculated $^{13}\Delta$ values from chamber measurements of environmental conditions, air composition and fluxes (see Appendix I) based on the three equations described next. Summary of symbols and definitions are given in Table 1. The most comprehensive ('classical') model of net ^{13}C discrimination ($^{13}\Delta_{classical}$, ‰) for C_3 plants describes our present understanding of fractionation steps during net assimilation of CO_2 (Farquhar *et al*. 1982) as

$$^{13}\Delta_{classical} = a_b\frac{C_a-C_s}{C_a} + a\frac{C_s-C_i}{C_a} + a_m\frac{C_i-C_c}{C_a} + b\frac{C_c}{C_a} - f\frac{\Gamma_*}{C_a} - e\frac{R_d}{kC_a} \qquad (3)$$

where a_b and a are the fractionations during diffusion of CO_2 in air through the leaf boundary layer and the stomata (≈ 2.9 and 4.4‰, Craig 1953), and b is the combined fractionation during carboxylation by ribulose 1,5-bisphosphate carboxylase/oxygenase (Rubisco) and phospho-enol-pyruvate carboxylase (PEPc) (assumed to be 29‰, Roeske & O'Leary 1984; Guy *et al*. 1989; Guy, Fogel & Berry 1993). a_m is the sum of the fractionation factors during internal CO_2 transfer, combining an equilibrium fractionation of CO_2 entering solution (e_s = 1.1‰ at 25 °C, Mook, Bommerson & Staverman 1974) and a diffusional fractionation of dissolved CO_2 in water (a_d = 0.7‰, O'Leary 1984). The respiratory fractionation factors are f for photorespiration (8 ± 1‰, Rooney 1988; Gillon & Griffiths 1997) and e for day respiration, R_d. C_c is the CO_2 mole fraction at the sites of carboxylation, k is the carboxylation efficiency and Γ_* is the CO_2 compensation point in the absence of day respiration.

Table 1. List of symbols used in the text

Symbols used in text		
A	Measured net rate of assimilation	μmol m^{-2} s^{-1}
A_{max}	Fitted maximum assimilation rate	μmol m^{-2} s^{-1}
a	^{13}C fractionation during diffusion through the stomata	4.4‰
a_b	^{13}C fractionation during diffusion through the boundary layer	2.9‰
a_d	^{13}C fractionation during diffusion through water	0.7‰
a_m	^{13}C fractionation during internal CO_2 transfer ($e_s + a_d$)	1.8‰
b	Net ^{13}C fractionation during carboxylation by ribulose 1,5-bisphosphate carboxylase/oxygenase and Phospho-enol-pyruvate carboxylase	29‰
$\bar{b}$	Estimated net ^{13}C fractionation during carboxylation, internal CO_2 transfer and decarboxylation	27‰
C_a	CO_2 mole fraction in ambient air	μmol mol^{-1}
C_c	CO_2 mole fraction at the sites of carboxylation	μmol mol^{-1}
C_e	CO_2 mole fraction of chamber air at the end of closure period	μmol mol^{-1}
C_i	CO_2 mole fraction in the intercellular spaces	μmol mol^{-1}
$C_{i,A}$	Assimilation weighted intercellular CO_2 mole fraction	μmol mol^{-1}
$C_{i,g}$	Conductance weighted intercellular CO_2 mole fraction	μmol mol^{-1}
C_o	CO_2 mole fraction of chamber air at the beginning of closure period	μmol mol^{-1}
C_s	CO_2 mole fraction at the leaf surface	μmol mol^{-1}
$^{13}\Delta$	Net discrimination against ^{13}C during photosynthesis	
$^{13}\Delta_{obs}$	Observed net ^{13}C discrimination (Eqn 2)	
$^{13}\Delta_{classical}$	Predicted net ^{13}C discrimination (Eqn 3, or eqn B24 of Farquhar *et al*. 1982)	
$^{13}\Delta_{pred}$	Predicted net ^{13}C discrimination	
$^{13}\Delta_{revised}$	Predicted net ^{13}C discrimination (Eqn 5)	
$^{13}\Delta_{simple}$	Predicted net ^{13}C discrimination (Eqn 4, or eqn 10 of Farquhar *et al*. 1982)	
$^{13}\Delta_R$	Carbon isotope signature of the respiratory flux (Eqn A2.10) defined as net respiratory discrimination in analogy to photosynthetic gas exchange	
$\delta^{13}C$	Carbon isotope composition ($\Re_{sample} / \Re_{standard} - 1) \times 1000$	‰
$\delta^{13}C_a$	Carbon isotope composition of ambient air	‰
$\delta^{13}C_{assimilates}$	Carbon isotope composition of assimilates	‰
$\delta^{13}C_e$	Carbon isotope composition of chamber air at the end of closure period	‰
$\delta^{13}C_{needle}$	Carbon isotope composition of bulk needle material	‰
$\delta^{13}C_o$	Carbon isotope composition of chamber air at the beginning of closure period	‰
$\delta^{13}C_{plant}$	Carbon isotope composition of bulk plant material	‰
$\delta^{13}C_R$	Carbon isotope composition of respired CO_2	‰
$\delta^{13}C_{substrate}$	Carbon isotope composition of substrate for dark respiration	‰
$\delta^{13}C_{wood}$	Carbon isotope composition of bulk twig material	‰
D_a	Vapour mole fraction deficit	mmol mol^{-1}
E	Transpiration rate	mol m^{-2} s^{-1}
e	^{13}C fractionation during decarboxylation	0 or –6‰
e_s	^{13}C fractionation during equilibration of CO_2 entering solution	1.1‰
e^*	Apparent discrimination against ^{13}C during decarboxylation ($= \Re_{substrate} / \Re_{assimilates} - 1$)	‰
f	Discrimination against $^{13}CO_2$ during photorespiration	8‰
g	Total branch conductance to water vapour	mol m^{-2} s^{-1}
g_b	Branch boundary layer conductance for CO2	1.1 mol m^{-2} s^{-1}
g_c	Branch conductance to CO_2	mol m^{-2} s^{-1}
g_i	Internal transfer conductance to CO_2	0.16 mol m^{-2} s^{-1}
g_s	Branch conductance to water vapour	mol m^{-2} s^{-1}
Γ_*	Temperature dependent CO_2 compensation point (Brooks & Farquhar 1985)	μmol mol^{-1}
h	Relative humidity	%
K	Carboxylation efficiency	mol m^{-2} s^{-1}
L_A	Projected needle area	m^2
P	Atmospheric pressure	Pa
Q	Photosynthetic photon flux density	μmol mol^{-1}
R_d	Measured rate of dark respiration	μmol m^{-2} s^{-1}
$R_{d,n}$	Estimated rate of day respiration, T dependent	μmol m^{-2} s^{-1}
$R_{d,i}$	Estimated rate of day respiration, T and Q dependent	μmol m^{-2} s^{-1}
$R_{d\,20}$	Fitted rate of dark respiration at 20 °C	μmol m^{-2} s^{-1}
$\Re_a$	Isotope (^{13}C) ratio of ambient CO_2	
$\Re_{assimilates}$	Isotope (^{13}C) ratio of assimilates	
$\Re_e$	Isotope (^{13}C) ratio of chamber air at end of closure period	
$\Re_o$	Isotope (^{13}C) ratio of chamber air at beginning of closure period	
$\Re_{standard}$	Isotope (^{13}C) ratio of V–PDB–CO_2 standard	
$\Re_{substrate}$	Isotope (^{13}C) ratio of substrate used for dark respiration	
T_a	Air temperature	°C
w_a	Air vapour mole fraction	mmol mol^{-1}
w_{a0}	Initial air vapour mole fraction in chamber at the starting time t_0	mmol mol^{-1}
$w_{a(h)}$	Air vapour mole fraction in chamber calculated from relative humidity	mmol mol^{-1}
$w_{a(corr)}$	Air vapour mole fraction corrected for the return flow of dry air during flask sampling	mmol mol^{-1}
w_i	Leaf vapour mole fraction	mmol mol^{-1}
V_a	Molar volume of air enclosed in the chamber	mol

The most often applied ('simple') model of ^{13}C discrimination ($^{13}\Delta_{simple}$) neglects any effects of photo- and day respiration on net discrimination, but implicitly accounts for transfer conductance by using a lower value for b (Farquhar *et al*. 1982; Farquhar & Richards 1984):

$$^{13}\Delta_{simple} = a + (\bar{b} - a)\frac{C_i}{C_a}, \quad (4)$$

where $\bar{b}$ is the weighted fractionation during internal transfer of CO_2 and fixation by RuP_2 and PEP carboxylases (27‰), applied to C_i (instead of C_c as in Eqn 3).

Equation 3 is based on the assumption that recent assimilates form the substrates of photorespiration and day respiration. This is likely to be the case for photorespiration as it recycles freshly assimilated carbon (Fig. 3). However, day respiration may also utilize other substrates, such as older carbohydrates (Schnyder *et al*. 2003; Nogués *et al*. 2004). If the $\delta^{13}C$ composition of these substrates is not the same as that of freshly assimilated carbon, the respiratory $\delta^{13}C$ signature would differ from instantaneous $^{13}\Delta$ by more than the fractionation factor (e). To take this effect into account, we incorporate an apparent fractionation for day respiration, e^*, defined as $e^* = \Re_{assimilates}/\Re_{substrate} - 1$, expressing the difference between the isotopic composition of the respiratory substrate ($\delta^{13}C_{substrate}$) and photosynthetic assimilates ($\delta^{13}C_{assimilate} \approx \delta^{13}C_a - {}^{13}\Delta$) at a given time, i.e. $e^* \approx \delta^{13}C_a - {}^{13}\Delta - \delta^{13}C_{substrate}$. This leads to the 'revised' model, a modified version of the classical model (Eqn 3, omitting boundary layer effects for clarity):

$$^{13}\Delta_{revised} = \frac{a + (a_m - a)\frac{C_i}{C_a} + (b - a_m)\frac{C_c}{C_a} - f\frac{\Gamma_*}{C_a} - \frac{(e + \delta^{13}C_a - \delta^{13}C_{substrate})\frac{R_d}{A + R_d}\frac{C_i - \Gamma_*}{C_a}}{1 - \frac{R_d}{A + R_d}\frac{C_i - \Gamma_*}{C_a}} \quad (5)$$

Alternatively, Eqn 6 retains the apparent factor e^* so that it can be easily compared to Eqn 3:

$$^{13}\Delta_{revised} = a_b\frac{C_a - C_s}{C_a} + a\frac{C_s - C_i}{C_a} + a_m\frac{C_i - C_c}{C_a} + b\frac{C_c}{C_a} - f\frac{\Gamma_*}{C_a} - (e + e^*)\frac{R_d}{kC_a} \quad (6)$$

The derivation of Eqns 5 and 6 are given in Appendix II (note that the $^{13}\Delta$ term of e^* is included in the left hand side of Eqn 5). When $\delta^{13}C_{substrate} = \delta^{13}C_{assimilate}$ (i.e. $e^* = 0$), Eqn 5 is again the classical Farquhar *et al*. (1982) description (Eqn 3).

In the following, we use the time series from the July campaign as an example to illustrate the different model predictions. Using Eqns 3, 4 and 5, $^{13}\Delta$ values were calculated and integrated over the chamber closure periods as described in Appendix I. Parameters required for the models are $\delta^{13}C_a$ from flask observations (i.e. $\delta^{13}C_o$), g_b, g_c and C_a from chamber measurements (see Methods), fractionation factors (a_b, a, a_m, b, f, e), and g_i, Γ_*, R_d and $\delta^{13}C_{substrate}$. The internal transfer conductance to CO_2 (g_i) was estimated from a linear regression of the difference between predicted $^{13}\Delta$ (Eqn 5 with infinite g_i) and $^{13}\Delta_{obs}$ against A/C_a (von Caemmerer & Evans 1991) using data from both months (not shown). The value obtained ($g_i = 0.16$ mol m^{-2} s^{-1}) was consistent with the relationship $g_i = 0.019 \cdot A_{max}$ (Warren *et al*. 2003) and A_{max} of 8.0 ± 1.5 μmol m^{-2} s^{-1} (obtained by fitting a non-rectangular hyperbola to the light response of branches).

The CO_2 compensation point in the absence of dark respiration, Γ_* (μmol mol^{-1}), was calculated from needle temperature (Farquhar & von Caemmerer 1982; Brooks & Farquhar 1985). Mitochondrial respiration associated with the tricarboxylic acid (TCA) cycle continues in the light, although it does not necessarily proceed at the same rate as that observed in the dark (Villar, Held & Merino 1994; Atkin *et al*. 2000; Tcherkez *et al*. 2005). To account for the potential range of day respiration rates, we calculated temperature-dependent rates (R_d) using R_{20} derived from nocturnal measurements (see Results section) and observed needle temperature, and based on these, light inhibited rates ($R_{d,i}$) as described by Lloyd *et al*. (1995). Day respiration was estimated to release 15% of gross photosynthetic CO_2 uptake during the day (only 4% for light-inhibited rate). During mornings and evenings, R_d and $R_{d,i}$ contributions were much larger (30 to 60%) while photorespiration was small (5 to 7%). Values of $\delta^{13}C_R$ measured for nocturnal respiration (Table 2) were used as estimates of $\delta^{13}C_{substrate}$ of day respiration in Eqn 5. We assumed that either 60 or 100% of day respiration was fed from this older substrate pool, with the remainder from newly assimilated carbon (Schnyder *et al*. 2003; Nogués *et al*. 2004). We used values of 0 and –6‰ for fractionation during day respiration (e) in Eqns 3 and 5 (see Discussion for a more detailed sensitivity analysis).

RESULTS

Diurnal patterns of branch microclimate and gas exchange

Daily time courses for environmental variables within branch chambers (at the beginning of chamber closure periods) are shown in Fig. 1. During May, direct beam irradiance dominated in the upper canopy, but in July, diffuse irradiance was persistent as indicated by low Q in the upper canopy (Fig. 1a,g). Marked diurnal patterns in air temperature (T_a) and vapour mole fraction deficit (D_a) were observed during both field campaigns (Fig. 1b,c,h,i). Temperatures were similar for both upper canopy chambers (1 and 3) during May and July, reaching 15 to 25 °C over the midday period (1000–1400 h), while T_a was lower in the middle canopy chamber (4) in May, ranging between 10 to 15 °C. Air vapour mole fraction deficits in May were higher than the values observed in the same chambers during July.

Table 2. The $\delta^{13}C$ of organic material collected in May 2001 at Griffin Forest, alongside the observed $\delta^{13}C_R$ signature of nocturnal branch respiration derived from mass balance, the assimilation-weighted composition of photoassimilates for the simple (Eqn 4), classical (Eqn 3) and revised models (Eqn 5) including the best fit parameter set for all branch chambers on 19 May and 20 July 2001

Sampling campaign, Canopy Location	Chamber	$\delta^{13}C_{needle} \pm 1SD$ (n) (‰)	$\delta^{13}C_{wood} \pm 1SD$ (n) (‰)	$\delta^{13}C_R \pm$ estimated uncertainty (‰)	Assimilation weighted daily $\delta^{13}C_{assimilates}$ and $^{13}\Delta$ (‰)			
					Simple model	Classical	Revised	Best fit
May, Upper	1	–29.0 ± 0.1 (4)	–27.7 ± 0.2 (4)	–27.7 ± 4.7	–26.1 (19.5)	–24.4 (17.7)	–24.3 (17.6)	–24.3 (17.6)
	3			–27.4 ± 5.8	–29.2 (22.7)	–29.9 (23.5)	–30.4 (24.0)	–30.9 (24.5)
May, Middle	4	–30.1 ± 0.3 (4)		–26.1 ± 13.0	–29.3 (22.8)	–28.0 (21.5)	–28.3 (21.8)	–28.6 (22.1)
May, Lower		–31.1 ± 0.1 (4)	–30.4 ± 0.0 (2)					
July, Upper	1			–25.2 ± 7.9	–25.5 (18.8)	–23.4 (16.7)	–23.6 (16.9)	–23.6 (16.9)
				–26.2 ± 1.8				
	3			–29.9 ± 8.5	–27.9 (21.3)	–25.9 (19.2)	–26.0 (19.3)	–26.0 (19.4)

Estimated uncertainties for $\delta^{13}C_R$ were calculated using data from a control branch chamber and Gaussian error propagation.

Daily time courses of gas exchange (beginning of closure periods) are also shown in Fig. 1. During May, assimilation rates (A) were highest before midday when Q was high and D_a was low, and were greater than in July (11 and 8 μmol m^{-2} s^{-1}, respectively, Fig. 1d,j). From 0900 to 1040 h and 1230 to 1500 h on 18 May 2001, technical difficulties in chambers 1 and 3 prevented determination of A, although all other measurements remained unaffected.

Values of branch conductance to water vapour (g_s) ranged between 100 and 250 mmol m^{-2} s^{-1} in the middle canopy and 30 to 170 mmol m^{-2} s^{-1} in the upper canopy during May (Fig. 1e), but values were much lower in July, between 50 and 150 mmol m^{-2} s^{-1} (Fig. 1k). Maximum g_s values were observed in the morning, subsequently declining over the day. The ratio of intercellular to ambient CO_2 mole fraction ($C_{i,g}/C_a$, conductance-weighted) during May remained between 0.4 to 0.8 for the upper canopy and 0.7 to 0.9 for the middle canopy (Fig. 1f). During July, $C_{i,g}/C_a$ was stable over most of the day and ranged between 0.5 and 0.8 for both upper branch chambers (Fig. 1l). However, as Q approached 0 during dawn and dusk, $C_{i,g}/C_a$ was typically 0.8 to 1. At dawn, the large $C_{i,g}/C_a$ occurred when values of A were low but g_s high. At dusk, high $C_{i,g}/C_a$ occurred primarily because of low A.

Nocturnal branch gas-exchange data for each chamber (Fig. 1d,j) were fitted with an Arrhenius type 'activation energy' response to needle temperature (e.g. Lloyd & Taylor 1994). The derived parameter, R_{20} (efflux rate at 20 °C) ranged from 2.5 to 3.3 μmol m^{-2} s^{-1} in May, and 1.3 to 1.4 μmol m^{-2} s^{-1} in July. Nocturnal branch respiration rates during May 2001 were larger than those observed in July 2001, even though temperatures were similar during the night.

Diurnal ^{13}C discrimination

We determined 22 values of ^{13}C discrimination during photosynthesis, $^{13}\Delta_{obs}$, from flask sample pairs (Eqn 2). During both field campaigns, we found a pronounced systematic diurnal variability in $^{13}\Delta_{obs}$ (Fig. 2). Highest $^{13}\Delta_{obs}$ occurred at dawn and dusk, ranging between 30 to 35‰. Around midday, $^{13}\Delta_{obs}$ were lowest at around 15‰. The middle canopy showed systematically higher $^{13}\Delta_{obs}$ than the upper canopy at similar times of the day. The highest daytime value (41‰) was measured in the mid canopy at noon in May. This and the high dusk and dawn values coincided with low net carbon and water vapour fluxes (Fig. 1). We also determined seven values for isotopic signatures of nocturnal foliage respiration, $\delta^{13}C_R$, from mass balances using flask samples pairs $[\delta^{13}C_R = (\delta^{13}C_eC_e - \delta^{13}C_oC_o) / (C_e - C_o)]$. Values of $\delta^{13}C_R$ in the upper canopy were more negative than in the middle canopy (Fig. 2). The latter was associated with a large uncertainty. For the same branch, $\delta^{13}C_R$ differed by nearly 2‰ between May and July. A relatively enriched $\delta^{13}C_R$ value of –19‰ was measured shortly before dawn during the July field campaign (Fig. 2b).

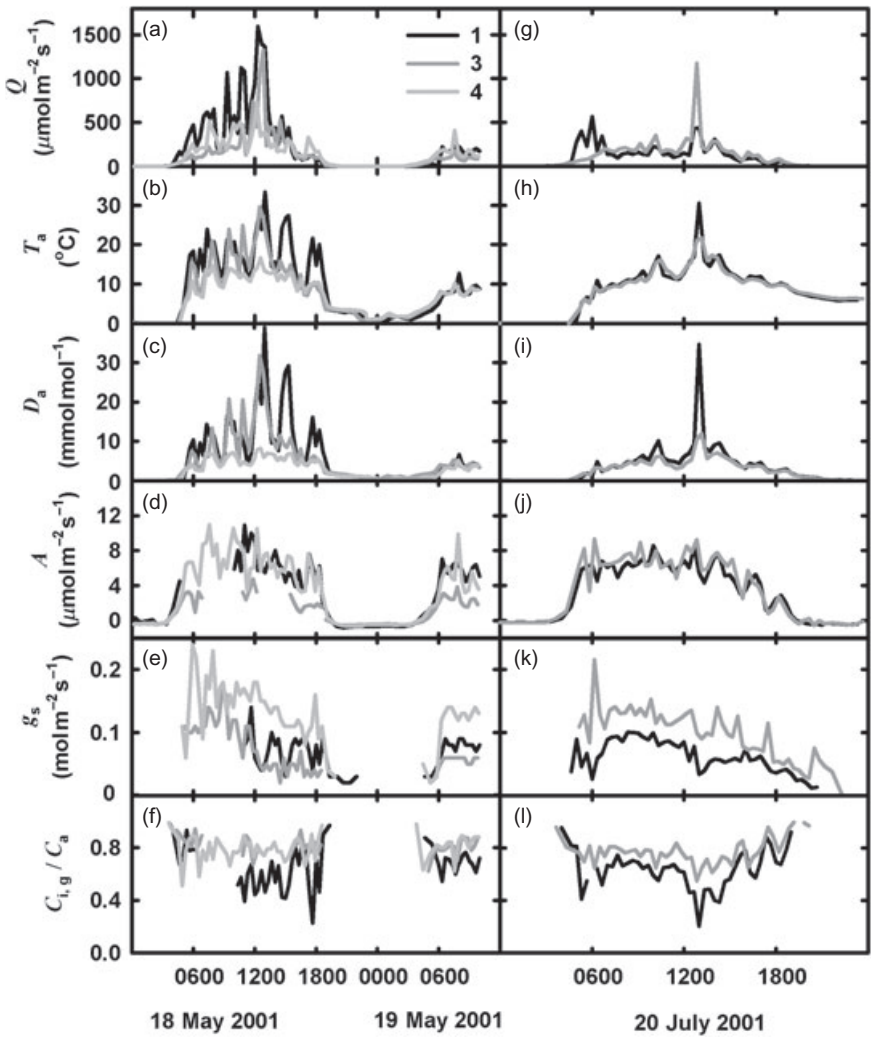

Figure 1. Daily variation of (a,g) photosynthetic photon flux density (Q), (b,h) air temperature (T_a), (c,i) air humidity deficit (D_a), (d,j) branch assimilation rate (A), (e, k) conductance to water vapour (g_s), and (f,l) conductance-weighted ratios of intercellular to ambient CO_2 mole fraction ($C_{i,g}/C_a$), measured every 20 min in branch chambers 1 (black), 3 (dark grey) and 4 (light grey) during May (a–f) and July (g–l) 2001.

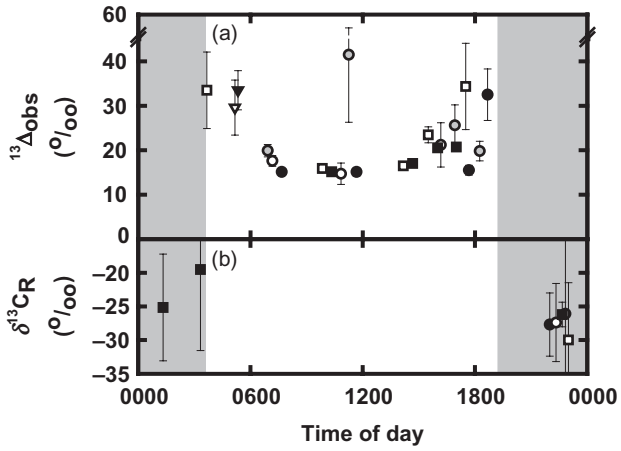

Figure 2. Diurnal variation in (a) observed net ^{13}C discrimination ($^{13}\Delta_{obs}$) and (b) the isotopic composition of dark respiration ($\delta^{13}C_R$) collected in different branch chambers (1: black, 3: white, 4: grey) during 18 (○) and 19 (▽) May 2001 and 20 July 2001 (□). Error bars indicate estimated uncertainties.

Predictions of $^{13}\Delta$ during foliage gas exchange

Photosynthetic ^{13}C discrimination calculated using the different models (Eqns 3–5) is presented in Fig. 4c together with the observations. As $^{13}\Delta_{simple}$ is linearly dependent on C_i/C_a and constrained by a and $\bar{b}$ (Eqn 4), the largest values predicted at dusk and dawn were 27‰, with most values between 16 and 22‰ for the rest of the day. In the afternoon, $^{13}\Delta_{simple}$ was close to $^{13}\Delta_{obs}$, indicating that during this period the actual drop between C_i and C_c may have corresponded to that implicitly included in $\bar{b}$ of Eqn 4. But at dusk and dawn, the observations exceeded the $^{13}\Delta_{simple}$ predictions consistently by up to 7‰ in both May (not shown) and July (Fig. 4c). Including additional effects in $^{13}\Delta_{classical}$ (Eqn 3), in particular those of internal CO_2 transfer when A was large during the day, improved the fit between predictions and observations (Fig. 4c). The contribution of photorespiration to net $^{13}\Delta$ values was generally less than 1‰, smaller than the effect including the internal conductance term, g_i (≈ 2‰). Using the largest negative fractionation reported for dark respiration so far (–6‰, Duranceau *et al*. 1999), the resulting contribution of

day respiration increased $^{13}\Delta_{classical}$ considerably but did not fully reconcile offsets between $^{13}\Delta_{classical}$ and $^{13}\Delta_{obs}$ at dusk and dawn. To illustrate the isotopic effect of day respiration on net $^{13}\Delta$ from the revised model (Eqn 5), the apparent fractionation factor (e^*) is shown in Fig. 4b. During the day, the calculated $\delta^{13}C$ signature of assimilates (e.g. $\delta^{13}C_a - {}^{13}\Delta \approx -25‰$) was close to that of the respiratory substrate ($\delta^{13}C_{substrate} \approx -26‰$, estimated from measurements of dark respiration), yielding small positive e^* values ($\approx 1‰$). Accordingly, day respiration had only minor effects on net $^{13}\Delta_{revised}$ values (Eqn 5) during most of the day (Fig. 4c). On the other hand, assimilates were substantially depleted ($\approx -36‰$) compared to the respiratory substrate ($-26‰$) at dusk and dawn, yielding large negative e^* values ($\approx -10‰$) at these times. The negative e^* together with high contributions of day respiration resulted in high $^{13}\Delta_{revised}$ at dusk and dawn comparable to the observations (Fig. 4c).

Values of $^{13}\Delta$ obtained from chamber integrations for the three modelling approaches ($^{13}\Delta_{pred}$) were compared with flask observations ($^{13}\Delta_{obs}$). The classical and revised models both improved the correlation between predicted and observed $^{13}\Delta$ values (Table 3). During the day, the classical and revised models predicted almost identical $^{13}\Delta$ values due to the generally small contribution of day respiration. But only the revised formulation showed reasonable agreement with the high $^{13}\Delta_{obs}$ at dusk and dawn (Fig. 5). Assuming that day respiration was fully supplied by 'old' substrates with a $\delta^{13}C$ signature equal to that measured at night, together with a fractionation factor (e) of $-6‰$, provided the highest correlation for our data set (Table 3).

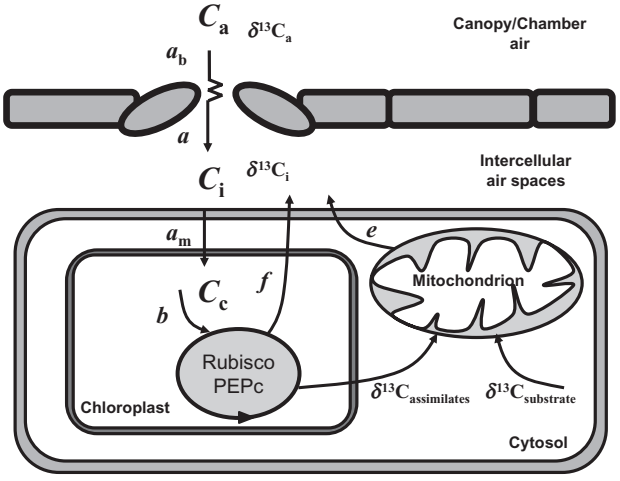

Figure 3. Conceptual diagram showing the flow of carbon during photosynthetic uptake and the fractionation factors associated with each part of the pathway: a_b for diffusion through the boundary layer, a for diffusion through stomata, a_m for internal CO_2 transfer, b for ribulose 1,5-bisphosphate carboxylase/oxygenase/phospho-enol-pyruvate carboxylase (Rubisco/PEPc) reactions, f for photorespiration and e for day (mitochondrial) respiration. Also shown are the CO_2 mole fractions (C_a, C_i, C_c) and the isotopic signatures of ambient CO_2, $\delta^{13}C_a$, and intercellular CO_2, $\delta^{13}C_i$, affected by the various fractionations during all CO_2 exchange processes, and those of newly assimilated carbohydrates, $\delta^{13}C_{assimilates}$, and other respiratory substrates, $\delta^{13}C_{substrate}$.

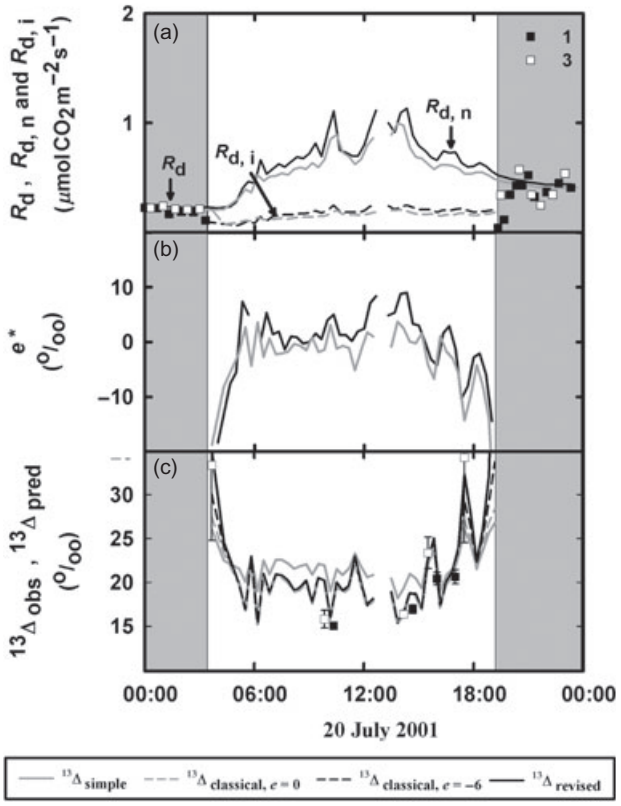

Figure 4. Daily variation in (a) observed dark respiration rates for each chamber (square symbols) (R_d), estimated rate of day respiration dependent on temperature ($R_{d,n}$ solid lines) and light-inhibited ($R_{d,i}$, dotted lines) for chambers 1 and 3 (black and grey lines, respectively), (b) the apparent fractionation factor, e^* for chambers 1 and 3 (black and grey lines) and (c) predicted $^{13}\Delta$ for chamber 3 from the simple model ($^{13}\Delta_{simple}$, Eqn 4, solid grey line), classical model ($^{13}\Delta_{classical}$, Eqn 3, assuming $e = 0$ or $e = -6‰$, dotted grey and black lines) and revised model ($^{13}\Delta_{revised}$, Eqn 5, solid black line) alongside net observed discrimination, $^{13}\Delta_{obs}$, for chambers 1 and 3 (black and white symbols) during 20 July 2001.

Daily foliage isofluxes and the $\delta^{13}C$ of organic matter

The aforementioned models of ^{13}C discrimination were applied to diurnal gas-exchange data (20 min time step) for the different branch chambers to yield diurnal variations of $^{13}\Delta$ expected in the absence of chambers. The $\delta^{13}C_a$ values, used in Eqn 5 and to compute $\delta^{13}C_{assimilates}$, were derived from a linear regression fitted to open branch chamber flask observations: May: $\delta^{13}C_a = 8194/C_a - 30.1‰$ ($r^2 = 0.91$, $n = 11$, $P < 0.0001$) and July: $\delta^{13}C_a = 6846/C_a - 26.5‰$ ($r^2 = 0.98$, $n = 9$, $P < 0.0001$), with daytime $\delta^{13}C_a$ variations of less than 1‰ for both field campaigns. Assimilation weighted diurnal average $^{13}\Delta$ and the corresponding $\delta^{13}C_{assimilates}$ values were then calculated for each

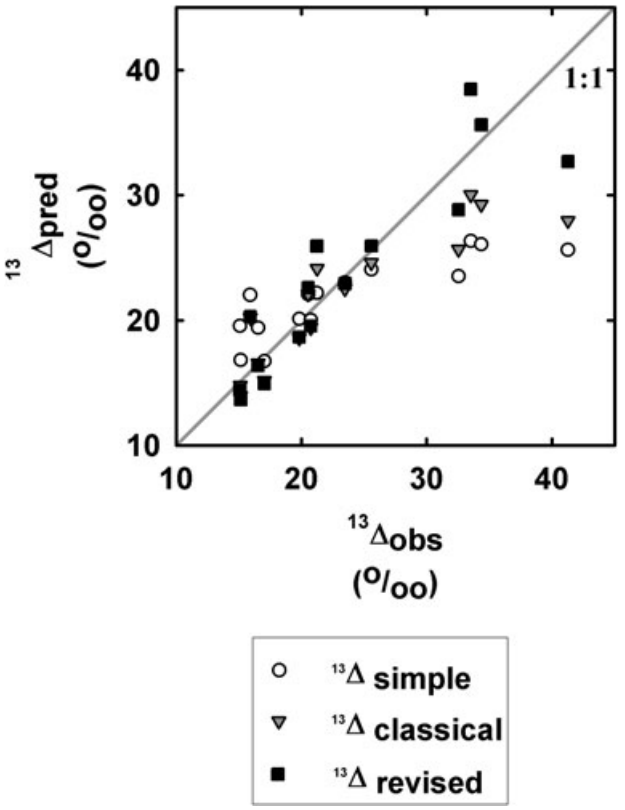

Figure 5. Observed ($^{13}\Delta_{obs}$) and predicted ($^{13}\Delta_{pred}$) discrimination against ^{13}C using the simple (Eqn 4), classical (Eqn 3) and revised models (Eqn 5) for all branch chambers during May and July 2001.

branch chamber and month (Table 2). The simple model predicted a 0.7–2.1‰ higher average $^{13}\Delta$ than the classical and revised models, and a correspondingly depleted $\delta^{13}C_{assimilates}$ of daily assimilated plant material. For all models, $\delta^{13}C_{assimilates}$ were enriched relative to $\delta^{13}C_{needle}$ for chambers 1 and 4, but similar for chamber 3. There were no consistent offsets between $\delta^{13}C_{assimilates}$ and $\delta^{13}C_R$ signatures of nocturnal respiration. For chamber 1, $\delta^{13}C_{assimilates}$ were enriched relative to $\delta^{13}C_R$, but depleted for chambers 3 and 4.

The $\delta^{13}C$ values of foliage ($\delta^{13}C_{needle}$) and woody ($\delta^{13}C_{wood}$) material in the upper canopy were typically enriched by 2 to 3‰ relative to lower canopy values (Table 2). This translates to a vertical gradient of 0.5‰ decrease in $\delta^{13}C_{needle}$ for every meter down the canopy profile ($r^2 = 0.9, n = 17, P < 0.0001$). We found that $\delta^{13}C_R$ was similar to $\delta^{13}C_{wood}$ but enriched relative to $\delta^{13}C_{needle}$ (2 to 4‰). This is consistent with many other observations (see Badeck *et al*. 2005 for review), however, we emphasize that the organic material was not collected from the branches measured for gas exchange, and that large uncertainties were associated with measurements at low flux rates (Table 2).

DISCUSSION

Our study aimed to characterize the diurnal patterns of $^{13}\Delta_{obs}$ during photosynthesis of *P. sitchensis* branches in the field (Fig. 2), and to explore how important internal CO_2 transfer, photorespiration and day respiration (see Fig. 3) were in shaping these patterns (Fig. 4). We measured $^{13}\Delta_{obs}$ over several diurnal periods on whole branches of *P. sitchensis*. We found a range of 15 to 41‰, comparable to that reported for a leaf scale study on *Piper aduncum* in a tropical forest of Trinidad (Harwood *et al*. 1998). Despite the differences in ecosystem and plant type, a similar diurnal pattern was observed in both studies: high $^{13}\Delta_{obs}$ values in the morning and low values around midday. Harwood *et al*. (1998) also documented large $^{13}\Delta_{obs}$ values at dawn. The observations reported in our and previous studies (Gillon *et al*. 1997; Harwood *et al*. 1998) were not captured by the commonly used simple Farquhar *et al*. (1982) model because it expresses $^{13}\Delta$ as a linear function of C_i/C_a alone (Eqn 4) and does not account explicitly for the various processes concurrently contributing to the net photosynthetic flux. In contrast, $^{13}\Delta_{obs}$ values were described well during most of the day by the classical Farquhar *et al*. (1982) model (Eqn 3) that incorporates photorespiration, day respiration and the diffusion of CO_2 to the site of carboxylation through a series of resistances. But the surprisingly large $^{13}\Delta_{obs}$ values at dawn and dusk systematically observed in our study (and by Harwood *et al*. 1998) could not be reconciled using Eqn 3.

It seems unlikely that the difference between predicted $^{13}\Delta$ and $^{13}\Delta_{obs}$ was due to erroneous assumptions for the parameters f and g_i. Both tend to decrease $^{13}\Delta$, and neither has large effects at dawn and dusk. Secondly, any alteration

Table 3. Regression output parameters between predicted and observed discrimination using the simple (Eqn 4), classical (Eqn 3) and revised models (Eqn 5) for all branch chambers during May and July 2001

Model	Parameters and values assigned							Slope	Int	*RMSE*
	b	*f*	*e*	g_w	R_d %	*e**	$R_{d,n}$ or $R_{d,i}$			
Simple (Δ_{simple})	27	–	–	–	0	–	–	0.28	16.3	6.1
Classical ($\Delta_{classical}$)	29	8	0	0.16	0	–	$R_{d,n}$	0.54	8.2	5.7
–Light inhibited	29	8	0	0.16	0	–	$R_{d,i}$	0.54	8.2	5.7
Classical ($\Delta_{classical}$)	29	8	–6	0.16	0	–	$R_{d,n}$	0.61	7.9	5.0
–Light inhibited	29	8	–6	0.16	0	–	$R_{d,i}$	0.58	7.8	5.4
Revised ($\Delta_{revised}$)	29	8	–6	0.16	60	Var	$R_{d,n}$	0.76	5.0	4.5
–Light inhibited	29	8	–6	0.16	60	Var	$R_{d,i}$	0.62	7.1	5.2
Best Fit	29	8	–6	0.16	100	Var	$R_{d,n}$	0.95	0.8	4.2

in either of these would also affect all other $^{13}\Delta$ predictions, and even increasing $^{13}\Delta$ to the limits of *b* by adopting an infinite g_i cannot explain all $^{13}\Delta_{obs}$ values. To attribute the large dusk and dawn $^{13}\Delta_{obs}$ primarily to fractionation by Rubisco, we would require a *b* value of at least 34‰. The value determined for Rubisco fractionation *in vitro* is ≈ 30‰ (Roeske & O'Leary 1984; Guy *et al*. 1987), with the additional contributions of PEP carboxylase typically decreasing the overall fractionation during carboxylation by 0.7 to 1.4‰. Apparent values of *b* were found between 27‰ for rice and radish and 32‰ for wheat (von Caemmerer & Evans 1991), hence, it is unknown how realistic a *b* of 34‰ is. On the other hand, changing *b* would increase $^{13}\Delta$ predictions over the whole diurnal cycle and thus require a concurrent decrease in our estimate of g_i by one third (to 0.1 mol m^{-2} s^{-1}) to recover the midday $^{13}\Delta_{obs}$ values. Transfer conductances of 0.1 to 0.2 mol m^{-2} s^{-1} have been observed for woody species (von Caemmerer & Evans 1991; Lloyd *et al*. 1992; Loreto *et al*. 1992; Epron *et al*. 1995; Warren *et al*. 2003). Temperature-related fluctuations in g_i (Bernacchi *et al*. 2002) were probably negligible because of the conservative temperature range during flask sampling. However, recalculations of the classical model incorporating a *b* of 34‰ and g_i of 0.1 mol m^{-2} s^{-1} still underestimated the dusk and dawn values by 3 to 5‰.

The assumption incorporated in the classical model (Eqn 3) is that day respiration utilizes recently synthesized carbohydrates, with a $\delta^{13}C$ signature indistinguishable from that of the concurrent net assimilation flux. Hence, day respiration affects $^{13}\Delta_{classical}$ (Eqn 3) only if there is fractionation (*e*) during this process. Estimates of fractionation during dark respiration range from 6 to –6 ‰ (Duranceau *et al*. 1999; Ghashghaie *et al*. 2003), but these might not be valid for day respiration (Tcherkez *et al*. 2004). However, we would need unrealistic values of *e* (up to –20‰) compared to the effects of much lower *e* values shown in Fig. 6a to explain $^{13}\Delta_{obs}$ purely based on fractionation during day respiration. Thus, recently synthesized carbohydrates may not constitute the only substrate for day respiration of *P. sitchensis* branches.

For dark respiration, older carbon pools may provide as much as 60% of the substrate (Schnyder *et al*. 2003; Nogués *et al*. 2004). Mitochondrial respiration is likely to utilize different substrates over time (Gleixner & Schmidt 1996; Schnyder *et al*. 2003; Tcherkez *et al*. 2003; Nogués *et al*. 2004; Prater, Mortazavi & Chanton 2006). Substrate shifts could occur between day and night in response to light-activated changes in metabolic pathways (Atkin *et al*. 2000; Tcherkez *et al*. 2005). In addition, these pathways may be affected by the non-statistical distribution of ^{13}C in carbohydrates (Gleixner & Schmidt 1996) or differ in isotope fractionation during the reactions themselves (Ghashghaie *et al*. 2003; Tcherkez *et al*. 2003). If day respiration utilizes carbon pools other than recently synthesized carbohydrates, its isotopic signature could differ from that of the concurrent assimilation flux (even for $e = 0$). This would create 'isotopic singularities', with extremely enriched or depleted $^{13}\Delta$ and $\delta^{13}C_R$ values as the net flux approaches zero. Such extreme values are the result of interpreting two opposing fluxes of similar magnitude with different isotopic signatures as a single net flux with a combined 'apparent' isotopic signature. Similar analyses of apparent isotopic signatures of net

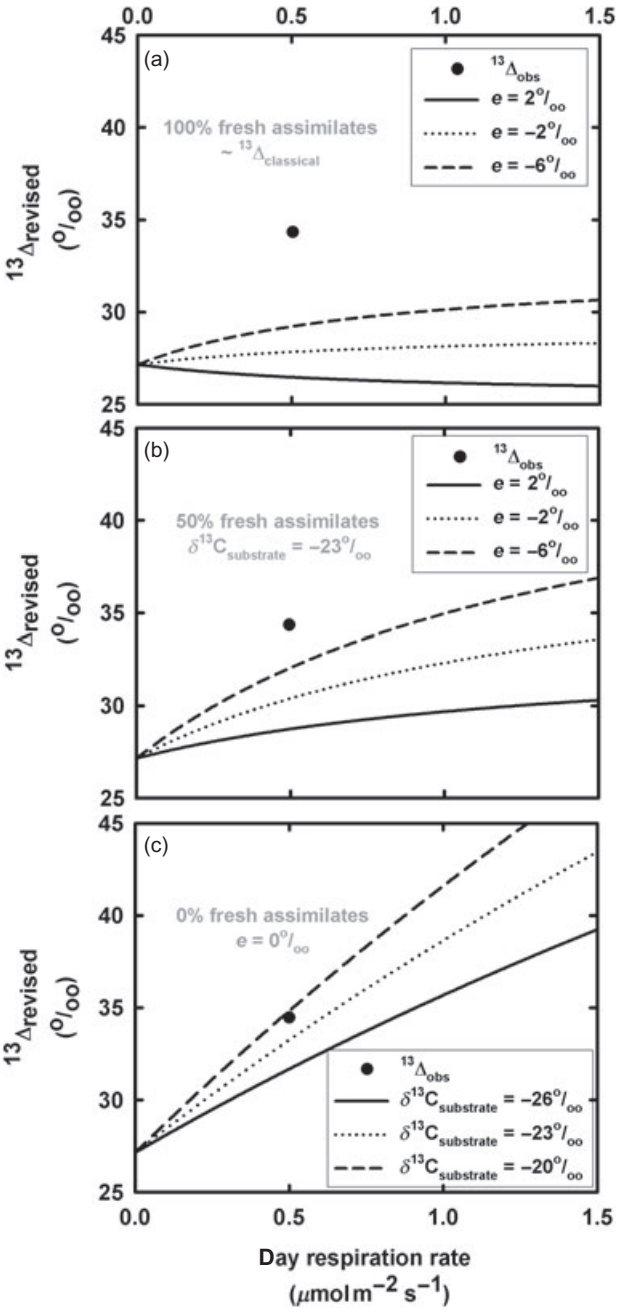

Figure 6. Sensitivity of $^{13}\Delta_{revised}$ (Eqn 5) to parameter assumptions relating to day respiration assuming (a) different values for *e* and using only fresh assimilates ≈ $^{13}\Delta_{classical}$ (Eqn 3), (b) different values for *e* and using 50% fresh assimilates and 50% old substrate, and (c) different values for $\delta^{13}C_{substrate}$, using only old substrate and an *e* of 0‰. The example chosen here was the high dusk value in July 2001, with $^{13}\Delta_{obs} = 34.4$‰, $Q = 36$ μmol m^{-2} s^{-1}, $g_s = 0.1$ mmol m^{-2} s^{-1}, $A = 0.8$ μmol m^{-2} s^{-1}, $R_d = 0.5$ μmol m^{-2} s^{-1}, $C_a = 360$ μmol mol^{-1}, $C_c = 341$ μmol mol^{-1}, $\delta^{13}C_a = -7.5$‰, $\delta^{13}C_{substrate} = -23$‰.

Table 4. Effects of averaging over different needle age classes on the value predicted for $^{13}\Delta$

Age class	L_A (% of total)	A (% of current)	g_s (% of current)	Predicted $^{13}\Delta$ (‰)	A weighted $^{13}\Delta$ (‰)	Difference g_s – A weighted $^{13}\Delta$ (‰)
Current	66	100	100	16.7	15.7	0.3
Current + 1	30	56	39	12.2		
Current + 2	4	54	40	13.1		
Branch total	L_A (cm^2)	A ($\mu mol\ m^{-2}\ s^{-1}$)	g_s ($mol\ m^{-2}\ s^{-1}$)	g_s weighted $^{13}\Delta$(‰)	$^{13}\Delta_{obs}$ (‰)	Difference g_s weighted – $^{13}\Delta_{obs}$ (‰)
	3842	4.31	0.025	16.0	17.0	–1.0

Relative needle area (L_A), assimilation rate (A) and stomatal conductance (g_c) for three different needle age classes, and their total values for the whole branch, with $^{13}\Delta$ values predicted for each age class separately and for the whole branch. The conductance-weighted age class average $^{13}\Delta$ corresponds to that calculated from branch total values, i.e. from gas-exchange measurements. The assimilation-weighted age class average $^{13}\Delta$ corresponds to that expected from isotope measurements.

fluxes have been presented at large scales for ^{13}C (Miller & Tans 2003; Helliker *et al*. 2005), and at the leaf scale for ^{13}C (Seibt 2003; Wingate 2003) and ^{18}O (Cernusak *et al*. 2004).

Here, we incorporated the opposing flux of day respiration into the equation for net ^{13}C discrimination (Eqn 5) to account for the mixing and recycling of respired CO_2 within the intercellular spaces in the same way as for photorespiration (see Fig. 3 & Appendix II). For example, using the fluxes associated with the large dusk $^{13}\Delta_{obs}$ in July 2001, (34.4‰, measured net A of 0.8 $\mu mol\ m^{-2}\ s^{-1}$, estimated $R_d \approx 0.5\ \mu mol\ m^{-2}\ s^{-1}$, correspondingly higher gross photosynthetic rate), calculations without recycling (eqn 7 of Miller & Tans 2003) predicted ≈ 1‰ larger net $^{13}\Delta$ than Eqn 5 for identical $\delta^{13}C$ signatures of the two gross fluxes. Incorporating an isotopically different substrate for day respiration, Eqn 5 thus can explain the large net $^{13}\Delta_{obs}$ values at dawn and dusk that could not be resolved by either of the other models (Eqns 3 & 4). Alternatively, the elevated $^{13}\Delta_{obs}$ can be thought of as reflecting a residual isoflux composed of the rate of day respiration, the $\delta^{13}C$ signature of the respiratory substrate and the fractionation. Very large absolute values of e are required if the substrate is assumed identical to newly assimilated carbohydrates. Smaller e values are needed the more the respiratory substrate differs from recent assimilates, and the larger the relative contribution of this substrate is (see Fig. 6). The respiratory isoflux thus contains too many unknowns to be decomposed without independent knowledge of its components. Ultimately, this can only be addressed through controlled laboratory and field measurements.

For the low $^{13}\Delta$ values usually coinciding with high A, Q and T, there was little difference between the classical and revised formulations. The slightly higher values of the classical model fitted the observed data better than our revised description. As the day respiration term is the only difference between the two models, this might indicate that the revised version overestimates the day respiratory contribution at these times. This could be resolved easily by assuming stronger inhibition of day respiration at high light and/or temperature levels (Atkin *et al*. 2000). Such a variable day respiration rate, contributing more at dawn and dusk and less during the rest of the day, would explain the observed diurnal pattern of $^{13}\Delta$ including the high dusk and dawn values. This scenario does not rule out, but also does not depend on, additional shifts in respiratory substrates, such as two similar but opposite substrate switches, one at dawn, the other at dusk, to explain the high $^{13}\Delta$ values observed at both times.

Lastly, we note that in our gas-exchange calculations, the foliage in the chambers was treated as a big leaf. However, enclosing whole branches meant that chamber measurements included the gas exchange of different aged needle cohorts, as well as contributions from woody material. Flask measurements provide assimilation-weighted $^{13}\Delta$ values, whereas gas-exchange measurements give conductance-weighted values for different age classes. Potential age class-related weighting effects on $^{13}\Delta$ (see Appendix III) are illustrated in Table 4. In addition, we calculated rates of woody respiration based on temperature measurements (Bosc, de Grandcourt & Loustau 2003). Woody respiration was estimated to contribute about 10% to day respiration rates at low light, i.e. less than 5% of photosynthetic foliage fluxes (even less during the rest of the day), due to the small ratio of stem/twig to foliage area. Therefore, the contributions of woody tissue fluxes to net CO_2 exchange and $\delta^{13}C$ fractionation observed in this study were considered negligible and ignored in the calculations detailed in Appendix I.

At larger spatial and temporal scales, the isotopic effects of day respiration can probably be neglected as the net flux of CO_2 during dusk and dawn periods represents such a small contribution to the daily flux weighted $^{13}\Delta$ signal. However, considering the increasing temporal resolution of $\delta^{13}C$ measurements (Bowling *et al*. 2001; Ogée *et al*. 2003, 2004; Knohl & Buchmann 2005), in particular, the high-resolution isotopic time series constructed using tunable diode laser absorption spectrometry (TDLAS) technology (Bowling *et al*. 2003; Griffis *et al*. 2005), we are increasingly likely to directly encounter the isotopic contributions from day respiration during leaf and ecosystem

scale studies. We also hypothesize that these respiratory signals could be more pronounced during periods of high meristematic activity, for instance, during shoot elongation [see, e.g. the increased R_d values in May (Table 2) associated with bud swelling]. During tissue growth in temperate species, storage carbohydrates such as starch are re-mobilized to provide metabolic energy at times of high demand. In the case of evergreen species such as *P. sitchensis*, these starch reserves accumulate during favourable environmental conditions over the winter (Bradbury & Malcolm 1978), whereas for deciduous species, they are accumulated towards the end of the previous year's growing season. These reserves could then contribute their distinct isotopic signatures to day respiration and, hence, net ^{13}C discrimination. The revised model (Eqn 5) presented here, together with detailed studies of metabolic cycling and storage in plants, will enable us to explain the resulting field observations of net $^{13}\Delta$. At the same time, high-resolution field data on $\delta^{13}C$ signatures of CO_2 fluxes during the light and dark will enable us to address some of the hypotheses and uncertainties highlighted in our study, and to make use of the potentially valuable information on C metabolism contained in photosynthetic isotope signals.

CONCLUSIONS

Our study highlights isotopic disequilibria during net ^{13}C discrimination leading to pronounced diurnal variability of $^{13}\Delta_{obs}$ in the field. The results of our study also emphasize the need for independent observations of transfer conductance to CO_2, as well as studies on the potential variability of b among and within species. With better constraints on the most critical parameters (g_i and b), observations of $^{13}\Delta$ and metabolite composition under controlled experimental conditions could allow us to indirectly probe respiratory signals during the light using stable carbon isotopes as tracers.

ACKNOWLEDGMENTS

We thank H. Geilmann, A. Jordan, M. Rothe and R. Werner for analysis of air and organic samples at the Max Planck Institute for Biogeochemistry, Jena and R. Clement, V. Finlayson, S. Patiño, F. Ripullone, J. Schmerler and A. Zerva for assistance in the field. We also thank Tilhill Economic Forestry for allowing us the use of Griffin Forest for this study. We are grateful to J. Kaplan, H. Griffiths, W.A. Brand, C. Jeffree, M.B. Rayment, J. Massheder, J. Grace, J. Severinghaus and S.C. Wong for their advice and/or loan of equipment during this project. We also thank M. Heimann, M. Mencuccini and J. Berry for continued support and discussions. Special thanks to J. Ogée for his input on an earlier draft and checking the derivation presented in Appendix I. This work was supported by a Natural Environment Research Council studentship (Ref No. GT04/98/93/TS) granted to L. Wingate and the EU-funded CARBOEUROFLUX projects (EC CT95-0078 and EC EVK2-CT-1999-00032), and by a Marie Curie International Fellowship (MOIF-CT-2004-2704) granted to U. Seibt. Lastly, we are grateful to the helpful comments provided by the anonymous reviewers that led to an improved version of the manuscript.

REFERENCES

Atkin O.K., Evans J.R., Ball M.C., Lambers H. & Pons T.L. (2000) Leaf respiration of Snow gum in the light and dark. Interactions between temperature and irradiance. *Plant Physiology* **122,** 915–923.

Badeck F.-W., Tcherkez G., Nogués H., Piel C. & Ghashghaie J. (2005) Post-photosynthetic fractionation of stable carbon isotopes between plant organs – a widespread phenomenon. *Rapid Communications in Mass Spectrometry* **19,** 1381–1391.

Barton C. (1997) *Effects of elevated atmospheric carbon dioxide concentration on growth and physiology of Sitka spruce [*Picea sitchensis *(Bong.) Carr*]. PhD thesis, University of Edinburgh, Edinburgh, UK.

Bernacchi C.J., Portis A.R., Nakano H., von Caemmerer S. & Long S.P. (2002) Temperature response of mesophyll conductance. Implications for the determination of rubisco enzyme kinetics and for limitations to photosynthesis in vivo. *Plant Physiology* **130,** 1992–1998.

Bosc A., de Grandcourt A. & Loustau D. (2003) Variability of stem and branch maintenance respiration in a Pinus pinaster tree. *Tree Physiology* **23,** 227–236.

Bowling D.R., Tans P.P. & Monson R.K. (2001) Partitioning net ecosystem carbon exchange with isotopic fluxes of CO_2. *Global Change Biology* **7,** 127–145.

Bowling D.R., Sargent S.D., Tanner B.D. & Ehleringer J.R. (2003) Tunable diode laser absorption spectroscopy for stable isotope studies of ecosystem-atmosphere CO_2 exchange. *Agricultural and Forest Meteorology* **116,** 159–179.

Bowling D.R., Burns S.P., Conway T.J., Monson R.K. & White J.W.C. (2005) Extensive observations of CO_2 carbon isotope content in and above a high-elevation subalpine forest. *Global Biogeochemical Cycles* **19,** GB3023. doi:10.1029/2004GB002394

Bradbury I.K. & Malcolm D.C. (1978) Dry matter accumulation by *Picea sitchensis* seedlings during winter. *Canadian Journal of Forest Research* **8,** 207–213.

Brooks A. & Farquhar G.D. (1985) Effect of temperature on the CO_2/O_2 specificity of ribulose 1,5-bisphosphate carboxylase oxygenase and the rate of respiration in the light: estimates from gas exchange measurements on spinach. *Planta* **165,** 397–406.

von Caemmerer S. & Evans J.R. (1991) Determination of the average partial pressure of CO_2 in chloroplasts from leaves of several C_3 plants. *Australian Journal of Plant Physiology* **18,** 287–305.

von Caemmerer S. & Farquhar G. (1981) Some relationships between the biochemistry of photosynthesis and the gas exchange of leaves. *Planta* **153,** 376–387.

Cernusak L.A., Farquhar G.D., Wong S.C. & Stuart-Williams H. (2004) Measurement and interpretation of the oxygen isotope composition of carbon dioxide respired by leaves in the dark. *Plant Physiology* **136,** 3350–3363.

Craig H. (1953) The geochemistry of the stable carbon isotopes. *Geochimica et Cosmochimica Acta* **3,** 53–92.

Duranceau M., Ghashghaie J., Badeck F., Deleens E. & Cornic G. (1999) $\delta^{13}C$ of CO_2 respired in the dark in relation to $\delta^{13}C$ of leaf carbohydrates in *Phaseolus vulgaris* L. under progressive drought. *Plant, Cell & Environment* **22,** 515–523.

Epron D., Godard D., Cornic G. & Genty B. (1995) Limitation of net CO_2 assimilation rate by internal resistances to CO_2 transfer

in the leaves of two tree species (*Fagus sylvatica* L. and *Castanea sativa* Mill.). *Plant, Cell & Environment* **18,** 43–51.

Farquhar G.D. (1989) Models of integrated photosynthesis of cells and leaves. *Philosophical Transactions of the Royal Society of London Series B-Biological Sciences* **323,** 357–367.

Farquhar G.D. & von Caemmerer S. (1982) Modelling of photosynthesis response to environmental conditions. In *Physiological Plant Ecology II: Water Relations & Carbon Assimilation* (eds O.L. Lange, P.S. Nobel, C.B. Osmond & H. Ziegler), pp. 549–587. Springer-Verlag, Berlin, Germany.

Farquhar G.D. & Richards R.A. (1984) Isotopic composition of plant carbon correlates with water use efficiency of wheat genotypes. *Australian Journal of Plant Physiology* **11,** 539–552.

Farquhar G.D., O'Leary M.H. & Berry J.A. (1982) On the relationship between carbon isotope discrimination and the intercellular carbon dioxide concentration in leaves. *Australian Journal of Plant Physiology* **9,** 121–137.

Francey R.J., Tans P.P., Allison C.E., Enting I.G., White J.W.C. & Trolier M. (1995) Changes in oceanic and terrestrial carbon uptake since 1982. *Nature* **373,** 326–330.

Ghashghaie J., Badeck F., Lanigan G. & Nogués S. (2003) Carbon isotope fractionation during dark respiration and photorespiration in C3 plants. *Phytochemistry Reviews* **2,** 145–161.

Gillon J.S. & Griffiths H. (1997) The influence of (photo) respiration on carbon isotope discrimination in plants. *Plant, Cell & Environment* **20,** 1217–1230.

Gillon J.S., Borland A., Harwood K.G., Roberts A., Broadmeadow M.S.J. & Griffiths H. (1997) Respiratory CO2 and instantaneous discrimination against 13C in plants: a source to be reckoned with? In *Stable Isotopes: Integration of Biological, Ecological and Geochemical Processes* (ed. H. Griffiths), pp. 111–132. Bios Scientific Publishers, Oxford, UK.

Gleixner G. & Schmidt H.-L. (1996) Carbon isotope effects on the fructose-1,6-bisphosphate aldolase reaction. Origin for non-statistical ^{13}C-distribution in carbohydrates. *Journal of Biological Chemistry* **272,** 5832–5387.

Griffis T.J., Baker J.M., Sargent S.D., Tanner B.D. & Zhang J. (2004) Measuring field-scale isotopic CO_2 fluxes with tunable diode laser absorption spectroscopy and micrometeorological techniques. *Agricultural and Forest Meteorology* **124,** 15–29.

Griffis T.J., Baker J.M. & Zhang J. (2005) Seasonal dynamics and partitioning of isotopic CO_2 exchange in a C3/C4 managed ecosystem. *Agricultural and Forest Meteorology* **132,** 1–19.

Guy R.D., Fogel M.L., Berry J.A. & Hoering T.C. (1987) Isotope fractionation during oxygen production and consumption by plants. In *Progress in Photosynthesis Research III* (ed. J. Biggins), pp. 597–600. Martinus Nijhoff, Dordrecht, the Netherlands.

Guy R.D., Berry J.A., Fogel M.L. & Hoering T.C. (1989) Differential fractionation of oxygen isotopes by cyanide-resistant and cyanide-sensitive respiration in plants. *Planta* **177,** 483–491.

Guy R.D., Fogel M.L. & Berry J.A. (1993) Photosynthetic fractionation of the stable isotopes of oxygen and carbon. *Plant Physiology* **101,** 37–47.

Harwood K.G. (1997) *Variation in the stable isotopes of oxygen and carbon within forest canopies*. PhD thesis, University of Newcastle-upon-Tyne, UK.

Harwood K.G., Gillon J.S., Griffiths H. & Broadmeadow M.S.J. (1998) Diurnal variation of $\Delta^{13}CO_2$, $\Delta C^{18}O^{16}O$ and evaporative site enrichment of $\delta H_2{}^{18}O$ in *Piper aduncum* under field conditions in Trinidad. *Plant, Cell & Environment* **21,** 269–283.

Helliker B.R., Berry J.A., Betts, A.K., Bakwin, P.S., Davis, K.J., Ehleringer, J.R., Butler, M.P. & Ricciuto D.M. (2005) Regional-scale estimates of forest CO2 and isotope flux based on monthly CO2 budgets of the atmospheric boundary layer. In *The Carbon Balance of Forest Biomes* (eds H. Griffiths and P.G. Jarvis), pp. 77–92. Taylor & Francis Group, Oxford, UK.

Jarman P.D. (1974) The diffusion of carbon dioxide and water vapour through stomata. *Journal of Experimental Botany* **25,** 927–936.

Knohl A.& Buchmann N. (2005) Partitioning the net CO_2 flux of a deciduous forest into respiration and assimilation using stable carbon isotopes. *Global Biogeochemical Cycles* **19,** GB4008. doi:10.1029/2004GB002301

Leverenz J., Deans J.D., Ford E.D., Jarvis P.G., Milne R. & Whitehead D. (1982) Systematic spatial variation of stomatal conductance in a Sitka spruce plantation. *Journal of Applied Ecology* **19,** 835–851.

Lloyd J. & Farquhar G.D. (1994) ^{13}C discrimination during CO_2 assimilation by the terrestrial biosphere. *Oecologia* **99,** 201–215.

Lloyd J. & Taylor J.A. (1994) On the temperature dependence of soil respiration. *Functional Ecology* **8,** 315–323.

Lloyd J., Syvertsen J.P., Kriedemann P.E. & Farquhar G.D. (1992) Low conductances for CO_2 diffusion from stomata to the sites of carboxylation in leaves of woody species. *Plant, Cell & Environment* **15,** 873–899.

Lloyd J., Grace J., Miranda A.C., Meir P., Wong S.C., Miranda B.S., Wright I.R., Gash J.H.C. & McIntyre J. (1995) A simple calibrated model of Amazon rain forest productivity based on leaf biochemical properties. *Plant, Cell & Environment* **18,** 1129–1145.

Lloyd J., Kruijt B., Hollinger D.Y., *et al*. (1996) Vegetation effects on the isotopic composition of atmospheric CO2 at local and regional scales: theoretical aspects and a comparison between rain forest in amazonia and a boreal forest in Siberia. *Australian Journal of Plant Physiology* **23,** 371–399.

Loreto F., Harley P.C., Di Marco G. & Sharkey T.D. (1992) Estimation of mesophyll conductance to CO_2 flux by three different methods. *Plant Physiology* **98,** 1437–1443.

Ludlow M.M. & Jarvis P.G. (1971) Photosynthesis in Sitka spruce [*Picea sitchensis* (Bong.) Carr.] I. General characteristics. *Journal of Applied Ecology* **8,** 925–953.

Miller J.B. & Tans P.P. (2003) Calculating isotopic fractionation from atmospheric measurements at various scales. *Tellus* **55,** 207–214.

Mook W.G., Bommerson J.C. & Staverman W.H. (1974) Carbon isotope fractionations between dissolved bicarbonate and gaseous carbon dioxide. *Earth and Planetary Science Letters* **22,** 169–176.

Nogués S., Tcherkez G., Cornic G. & Ghashghaie J. (2004) Respiratory carbon metabolism following illumination in intact French Bean leaves using ^{13}C/^{12}C isotope labelling. *Plant Physiology* **136,** 1–10.

Ogée J., Peylin P., Ciais P., Bariac T., Brunet Y., Berbigier P., Roche C., Richard P., Bardoux G. & Bonnefond J.-M. (2003) Partitioning net ecosystem exchange into net assimilation and respiration using $^{13}CO_2$ measurements: a cost-effective sampling strategy. *Global Biogeochemical Cycles* **17,** 1070. doi:1010.1029/2002BG001995

Ogée J., Peylin P., Cuntz M., Bariac T., Brunet Y., Berbigier P., Richard P. & Ciais P. (2004) Partitioning net ecosystem carbon exchange into net assimilation and respiration with canopy-scale isotopic measurements: an error propagation analysis with $^{13}CO_2$ and $CO^{18}O$ data. *Global Biogeochemical Cycles* **18,** GB2019. doi:10.1029/2003GB002166

O'Leary M.H. (1984) Measurement of the isotopic fractionation associated with diffusion of carbon dioxide in aqueous solution. *Journal of Physical Chemistry* **88,** 823–825.

Prater J.L., Mortazavi B. & Chanton J.P. (2006) Diurnal variation of the δ^{13}C of pine needle respired CO_2 evolved in darkness. *Plant, Cell & Environment* **29,** 202–211.

Randerson J.T., Collatz G.J., Fessenden J.E., Munoz A.D., Still C.J., Berry J.A., Fung I.Y., Suits N. & Denning A.S. (2002) A possible global covariance between terrestrial gross primary production and ^{13}C discrimination: consequences for the atmospheric ^{13}C budget and its response to ENSO. *Global Biogeochemical Cycles* **16,** 1136. doi:10.1029/2001GB001845

Rayment M.B. & Jarvis P.G. (1999) Seasonal gas exchange of black spruce using an automatic branch bag system. *Canadian Journal of Forest Research* **29L,** 1528–1538.

Roeske C.A. & O'Leary M.H. (1984) Carbon isotope effects on the enzyme-catalyzed carboxylation of ribulose bisphosphate. *Biochemistry* **23,** 6275–6284.

Rooney M.A. (1988) *Short-term carbon isotope fractionation by plants*. PhD thesis, University of Wisconsin, Madison, WI, USA.

Schnyder H., Schäufele R., Lötscher M. & Gebbing T. (2003) Disentangling CO_2 fluxes: direct measurements of mesocosm-scale natural abundance $^{13}CO_2/^{12}CO_2$ gas exchange, ^{13}C discrimination, and labelling of CO_2 exchange flux components in controlled environments. *Plant, Cell & Environment* **26,** 1863–1874.

Seibt U. (2003) *Processes controlling the isotopic composition of CO_2 and O_2 in canopy air: a theoretical analysis with some observations in a Sitka spruce plantation*. PhD thesis, University of Hamburg, Hamburg, Germany.

Seibt U., Brand W., Heimann M., Lloyd J., Severinghaus J.P. & Wingate L. (2004) Observations of O_2:CO_2 exchange ratios during ecosystem gas exchange. *Global Biogeochemical Cycles* **18,** GB4024. doi:10.1029/2004GB002242

Seibt U., Wingate L., Berry J. & Lloyd J. (2006) Non-steady state effects in diurnal ^{18}O discrimination by *Picea sitchensis* branches in the field. *Plant, Cell & Environment* **29,** 928–939.

Tans P.P., Berry J.A. & Keeling R.F. (1993) Oceanic $^{13}C/^{12}C$ observations: a new window on ocean CO_2 uptake. *Global Biogeochemical Cycles* **7,** 353–368.

Tcherkez G., Nogués S., Bleton J., Cornic G., Badeck F. & Ghashghaie J. (2003) Metabolic origin of carbon isotope composition of leaf dark-respired CO_2 in French bean. *Plant Physiology* **131,** 237–244.

Tcherkez G., Farquhar G., Badeck F. & Ghashghaie J. (2004) Theoretical considerations about carbon isotope distribution in glucose of C3 plants. *Functional Plant Biology* **31,** 857–877.

Tcherkez G., Cornic G., Bligny R., Gout E. & Ghashghaie J. (2005) *In vivo* respiratory metabolism of illuminated leaves. *Plant Physiology* **138,** 1596–1606.

Villar R., Held A.A. & Merino J. (1994) Comparison of methods to estimate dark respiration in the light in leaves of two woody species. *Plant Physiology* **105,** 167–172.

Wang Y.P. (1988) *Crown structure, radiation absorption, photosynthesis and transpiration*. PhD thesis, University of Edinburgh, Edinburgh, UK.

Warren C.R., Ethier G.J., Livingston N.J., Grant N.J., Turpin D.H., Harrison D.L. & Black T.A. (2003) Transfer conductance in second growth Douglas-fir [*Pseudotsuga menziesii* (Mirb.) Franco] canopies. *Plant, Cell & Environment* **26,** 1215–1227.

Watts W.R., Neilson R.E. & Jarvis P.G. (1976) Photosynthesis in Sitka spruce [*Picea sitchensis* (Bong.) Carr.] VII. Measurements of stomatal conductance and CO_2 uptake in a forest canopy. *Journal of Applied Ecology* **13,** 622–638.

Werner R.A., Rothe M. & Brand W.A. (2001) Extraction of CO_2 from air samples for isotopic analysis and limits to ultra high precision $\delta^{18}O$ determination in CO_2 gas. *Rapid Communications in Mass Spectrometry* **15,** 2152–2167.

Wingate L. (2003) *The contribution of photosynthesis and respiration to the net ecosystem exchange and ecosystem ^{13}C discrimination of a Sitka spruce plantation*. PhD thesis, University of Edinburgh, Edinburgh, UK.

Yakir D. & Wang X.F. (1996) Fluxes of CO_2 and water between terrestrial vegetation and the atmosphere estimated from isotope measurements. *Nature* **380,** 515–517.

Received 3 October 2006; received in revised form 12 December 2006; accepted for publication 22 December 2006

APPENDIX I: ANALYSIS OF CLOSED CHAMBER MEASUREMENTS

Gas exchange in closed chambers will lead to transient changes in micro-environmental conditions, air composition and fluxes during the closure period. Flask samples collected at the start and end of chamber closure periods integrate over such changes. Furthermore, the air flushed through the flasks and back into the chambers was dried, weakening the increase in chamber water vapour content. Here, we briefly describe how we take both into account when integrating chamber gas-exchange data (5 s time step) to obtain $^{13}\Delta$ predictions that are directly comparable to flask observations (see also appendix II of Seibt *et al*. 2006). The data processing described in the following (for chamber 1 on 20 July 2001, 1440 to 1445 h) was implemented in an IDL program.

During the 5 min chamber closure, photon flux density was 127 ± 3 μmol m^{-2} s^{-1}, and air and leaf temperatures were 14 ± 0.7 °C. We assumed that to a good approximation, stomatal conductance remained constant within this period (Ludlow & Jarvis 1971). Relative humidity data (h) were used to calculate the vapour mole fraction of the enclosed air [$w_{a(h)}$, Fig. 7a]. During flask sampling periods, the air vapour mole fraction was corrected for the flow of dry air (3 dm^3 min^{-1}) returned from the flask sampling system [$w_{a(corr)}$]. Assuming saturated air at leaf temperature yielded a leaf vapour mole fraction (w_i) of 16.4 mmol mol^{-1}. The total conductance to water vapour (g, 0.051 mol m^{-2} s^{-1} for this period) was obtained from the increase in air vapour mole fraction [$w_{a(corr)}$: 9 to 14 mmol mol^{-1}, h: 56 to 78%] by fitting

$$w_a = w_i + (w_{a0} - w_i)\, e^{-\frac{L_a}{V_a} g (t - t_0)} \qquad \text{(A1.1)}$$

to leaf and air vapour mole fraction data at time t during the closure periods, where w_{a0} is the initial air vapour mole fraction at the starting time t_0. L_a and V_a are the leaf area and air molar volume enclosed in the chamber and g represents the total conductance to water vapour combining boundary layer and stomatal components. The transpiration rate decreased from 0.4 to 0.1 mmol m^{-2} s^{-1} during the closure period. The CO_2 mole fraction of chamber air (C_a, Fig. 7b) decreased from 350 to 275 μmol mol^{-1}. The C_a data were fitted with a quadratic equation, its derivative yielding a linear approximation of A (most $R^2 > 0.99$). Because C_a and A varied concurrently, the change in C_i (Eqn 1, Fig. 7b) was weaker than that of C_a, leading to a small increase in C_i/C_a over the closure period (Fig. 7c).

Using the $\delta^{13}C_a$ values observed in the open chambers as starting point values, we then calculated $^{13}\Delta$ (Eqns 3–5) and a new $\delta^{13}C_{a(pred)}$ (Eqn 2) for each 5 s time step. These $^{13}\Delta$ and $\delta^{13}C_{a(pred)}$ values increased from 17 to 18‰ (Fig. 7c) and –7

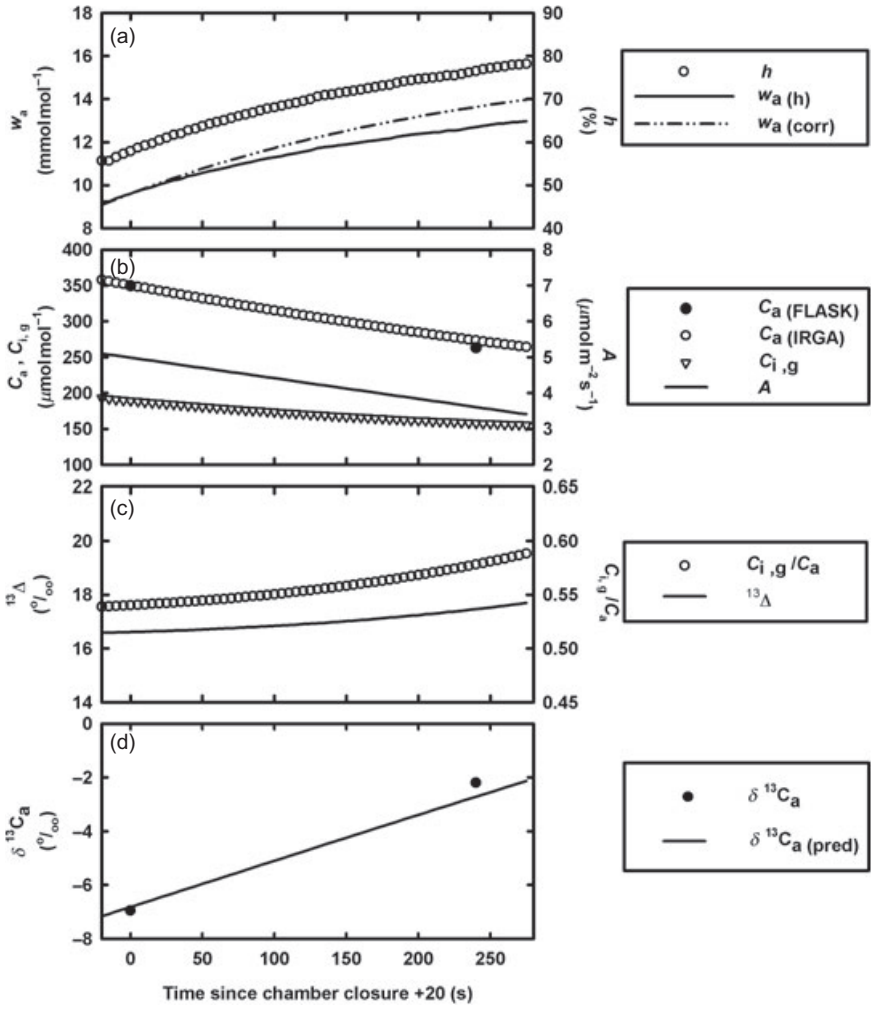

Figure 7. Changes in branch chamber 1 during the 5 min closure period at 1440 h on 20 July 2001: (a) observed relative humidity (h) and calculated air vapour mole fraction, uncorrected [$w_{a(h)}$] and corrected [$w_{a(corr)}$] for the recirculation of dried air by the sampling system; (b) CO_2 mole fraction observed by the infrared gas analyser (IRGA) [$C_{a(IRGA)}$] and flask sampling method [$C_{a(FLASK)}$], and calculated intercellular CO_2 mole fraction (C_i) and net assimilation rate (A); (c) calculated ratio of ambient to intercellular CO_2 mole fraction ($C_{i,g}/C_a$) and photosynthetic ^{13}C discrimination ($^{13}\Delta$), and (d) flask observed ($\delta^{13}C_a$) and calculated [$\delta^{13}C_{a\ (pred)}$] isotopic signature of chamber air.

to –2‰ (Fig. 7d) during the closure periods, respectively. Weighted averages of $\delta^{13}C_a$ and C_a were calculated from the time steps to reflect the air mixture collected in the 'closed' flask sample. Integrated $^{13}\Delta$ values were then obtained from $\delta^{13}C_a$ and C_a at the start and their weighted averages at the end of chamber closure periods using Eqn 2. This approach is equivalent to the calculations using flask data, making both methods directly comparable. For the example used here, the integrated $^{13}\Delta$ value of 16.9‰ was closer to the flask observed values of 17.0‰ than the starting point estimate of 16.6‰.

APPENDIX II: THE EFFECT OF DAY RESPIRATION ON NET DISCRIMINATION

Currently, the most complete, 'classical' model for net ^{13}C discrimination, $^{13}\Delta$, during photosynthesis of C_3 plants (Farquhar *et al*. 1982) accounts for fractionation (e) during day respiration (R_d) but assumes that current assimilates form its substrate (Eqn 3). In the following, we use a simplified version of Eqn 3 (see eqn B24 of Farquhar *et al*. 1982) omitting boundary layer and transfer conductances for clarity (the actual calculations always included all terms):

$$^{13}\Delta_{classical} = a + (b-a)\frac{C_i}{C_a} - f\frac{\Gamma_*}{C_a} - e\frac{R_d}{kC_a} \qquad (A2.1)$$

Here, we derive an equation for net photosynthetic ^{13}C discrimination that accounts for an isotopically distinct substrate used for day respiration. No specific assumption is made about the substrate and fractionation (e), which may come from various pools (sucrose, starch, lipids, etc.) with different metabolic pathways (Gleixner & Schmidt 1996; Schnyder *et al*. 2003; Tcherkez *et al*. 2003, 2004; Nogués *et al*. 2004). In the following, we use the notation of Farquhar *et al*. (1982), with B indicating equations from their appendix II. Using eqns B12, B12′, B18, B18′, B19 and B19′, the $^{13}\Delta$ of net assimilation (including photorespiration and daytime dark respiration) is given by

$$\frac{A'}{A} = (1-{}^{13}\Delta)\Re_a = \frac{g'}{g}\cdot\frac{g+kP}{g'+k'P}\cdot\frac{k'\left(C'_a-\Gamma'_*\right)-R'_d}{k\left(C_a-\Gamma_*\right)-R_d}, \qquad (A2.2)$$

where $\Re_a = C'_a/C_a$ denotes the isotope ratio of atmospheric CO_2, and P is atmospheric pressure. The fractionations

associated with diffusion (*a*, eqn B22), carboxylation (*b*, eqn B16) and photorespiration (*f*, eqn B5) are defined as in Farquhar *et al*. (1982). But the isotope ratio of recent assimilates (A'/A) in eqn B8 $[R'_d/R_d = (1-e)(A'/A)]$ is replaced by the isotope ratio of the substrate used for day respiration, $\Re_{substrate}$:

$$\frac{R'_d}{R_d} = (1-e)\Re_{substrate} \tag{A2.3}$$

Using the fractionation factors and $\Gamma'_*/\Gamma_* \approx (1 + b - {}^{13}\Delta - f)\cdot\Re_a$ (eqn B17) in Eqn A2.2 gives

$$(1-{}^{13}\Delta)\cdot\Re_a = (1-a)\cdot\frac{g+kP}{g(1-a)+kP(1-b)}\cdot \frac{k(1-b)\left(C_a-\Gamma_*-\Gamma_*(b-{}^{13}\Delta-f)\right)}{k\left(C_a-\Gamma_*\right)-R_d}\cdot \frac{\Re_a - R_d(1-e)\Re_{substrate}}{} \tag{A2.4}$$

Rearranging and neglecting second-order terms lead to the following expression:

$$\begin{aligned}(1-{}^{13}\Delta)\cdot\Re_a &\approx (1-a)\cdot\frac{g+kP}{g+kP-(ag+bkP)}\cdot \frac{\left[k\left(C_a-\Gamma_*\right)-R_d\right]\Re_a-\left[k\left(bC_a-({}^{13}\Delta+f)\Gamma_*\right)-R_d\right]\Re_a-R_d(1-e)\Re_{substrate}}{k\left(C_a-\Gamma_*\right)-R_d}\\ &\approx (1-a)\cdot\left(1+\frac{ag+bkP}{g+kP}\right)\cdot \left\{\Re_a-\frac{\left[k\left(bC_a-({}^{13}\Delta+f)\Gamma_*\right)-R_d\right]}{k\left(C_a-\Gamma_*\right)-R_d}\Re_a-\frac{R_d(1-e)}{k\left(C_a-\Gamma_*\right)-R_d}\Re_{substrate}\right\}\\ &\approx \left(1-a+\frac{ag+bkP}{g+kP}\right)\cdot\left\{1-b\frac{kC_a}{k\left(C_a-\Gamma_*\right)-R_d}+({}^{13}\Delta+f)\frac{k\Gamma_*}{k\left(C_a-\Gamma_*\right)-R_d}+e\frac{R_d}{k\left(C_a-\Gamma_*\right)-R_d}\frac{\Re_{substrate}}{\Re_a}-\frac{R_d}{k\left(C_a-\Gamma_*\right)-R_d}\left(\frac{\Re_{substrate}}{\Re_a}-1\right)\right\}\cdot\Re_a\\ &\approx \left\{1+\frac{kP}{g+kP}[b-a]-\frac{kC_a}{k\left(C_a-\Gamma_*\right)-R_d}\cdot\left[b-({}^{13}\Delta+f)\frac{\Gamma_*}{C_a}-e\frac{R_d}{kC_a}+\frac{R_d}{kC_a}\left(\frac{\Re_{substrate}}{\Re_a}-1\right)\right]\right\}\cdot\Re_a\end{aligned} \tag{A2.5}$$

Substituting $\frac{kP}{g+kP} = \frac{kC_a}{k\left(C_a-\Gamma_*\right)-R_d}\cdot\frac{C_a-C_i}{C_a}$ (eqns B12, B18 and B19), we get

$${}^{13}\Delta \approx \frac{kC_a}{k\left(C_a-\Gamma_*\right)-R_d}\left[a+(b-a)\frac{C_i}{C_a}-({}^{13}\Delta+f)\frac{\Gamma_*}{C_a}-e\frac{R_d}{kC_a}\frac{\Re_{substrate}}{\Re_a}+\frac{R_d}{kC_a}\left(\frac{\Re_{substrate}}{\Re_a}-1\right)\right] \tag{A2.6}$$

Because ${}^{13}\Delta$ appears on both sides of Eqn A2.6, we rearrange (neglecting second-order terms) to get the net ${}^{13}C$ discrimination for any dark respiratory substrate:

$${}^{13}\Delta_{revised} \approx \frac{kC_a}{k\left(C_a-\Gamma_*\right)-R_d}\left[a+(b-a)\frac{C_i}{C_a}-f\frac{\Gamma_*}{C_a}-(e+\delta^{13}\mathbf{C}_{atm}-\delta^{13}\mathbf{C}_{substrate})\frac{R_d}{kC_a}\right] \tag{A2.7}$$

If the substrate effect of dark respiration on net ${}^{13}C$ discrimination is expressed as apparent fractionation, $e^* \approx \delta^{13}C_{atm} - \delta^{13}C_{substrate} - {}^{13}\Delta$, i.e. the isotopic difference between dark respiration and photosynthesis, we can substitute $\Re_{substrate} = (1-e^*)\ (A'/A)$ in Eqn A2.3 to give $R'_d/R_d = [1-(e+e^*)](A'/A)$. Using this apparent factor e^*, Eqn A2.7 can be directly compared to Eqn A2.1:

$${}^{13}\Delta_{revised} = a+(b-a)\frac{C_i}{C_a}-f\frac{\Gamma_*}{C_a}-(e+e^*)\frac{R_d}{kC_a} \tag{A2.8}$$

If $\delta^{13}C_{substrate} = \delta^{13}C_{atm} - {}^{13}\Delta$ ($e^* = 0$), the revised equation (A2.7, A2.8 & A2.9) is again the classical model of Farquhar *et al*. (1982) as in Eqn A2.1.

Alternatively, the carboxylation efficiency k can be substituted in Eqn A2.7 using $k = (A + R_d)/(C_i - \Gamma_*)$ from appendix II, (Farquhar *et al*. 1982) to yield Eqn 5 of the main text, a useful version because it contains only variables that were measured in our study:

$${}^{13}\Delta_{revised} = \frac{a+(b-a)\frac{C_i}{C_a}-f\frac{\Gamma_*}{C_a}-(e+\delta^{13}C_{atm}-\delta^{13}C_{substrate})\frac{R_d}{A+R_d}\frac{C_i-\Gamma^*}{C_a}}{1-\frac{R_d}{A+R_d}\frac{C_i\,\Gamma^*}{C_a}} \tag{A2.9}$$

Lastly, in the absence of light, $k = 0$ and Eqn A2.7 reduces to

$${}^{13}\Delta_R \approx e - \delta^{13}C_{substrate} + \delta^{13}C_{atm}, \tag{A2.10}$$

demonstrating that in the absence of carboxylation, the $\delta^{13}C$ signature of the respiratory flux (${}^{13}\Delta_R$) with respect to the atmospheric composition is given by the respiratory substrate minus the fractionation factor (keeping the notation of Eqn A2.7, but *e* referring to dark respiration here). We therefore recommend the use of Eqn A2.7 instead of Eqn A2.1 because it is valid at any time of the day, even for dark respiration (J. Ogée, personal communication).

APPENDIX III: WEIGHTING OF GAS-EXCHANGE AND ISOTOPE MEASUREMENTS

The calculations of gas exchange in this study have effectively assumed the branch can be represented as a 'big leaf', despite the inclusion of multiple needle cohorts where uniform assimilation, stomatal and internal conductances are unlikely. The implications of such heterogeneity on the weighting of gas-exchange and isotope measurements have already been shown for individual leaves (Farquhar 1989; Lloyd *et al*. 1992) and plant canopies (Lloyd *et al*. 1996). Indeed, there are systematic differences in the gas-exchange characteristics of differing needle age classes for *P. sitchensis* (Ludlow & Jarvis 1971; Watts, Neilson & Jarvis 1976; Leverenz *et al*. 1982; Barton 1997). The presence of different needle age classes on the same branch thus represents a similar situation to that of stomatal heterogeneity for single leaves. Branches in our study contained a maximum of three age classes, with each age class transpiring and assimilating at different rates. Carbon isotope discrimination is carried by the net flux of CO_2, i.e. different age classes contribute to the average $^{13}\Delta$ according to their respective assimilation rates. Deriving C_i/C_a from flask $^{13}\Delta$ measurements thus provides an assimilation-weighted value of C_i ($C_{i,A}$). In contrast, different age classes contribute to the average C_i/C_a derived from IRGA gas-exchange data according to their respective stomatal conductances, i.e. gas-exchange measurements give a conductance-weighted value of C_i ($C_{i,g}$ see Eqn 1) (Farquhar 1989).

Potential age class-related weighting effects on $^{13}\Delta$ are illustrated in Table 4. Values of $^{13}\Delta$ were determined for each needle age class separately, based on variations of A and g_s observed across age classes for *P. sitchensis* (Ludlow & Jarvis 1971). Assimilation and conductance weighted $^{13}\Delta$ averages for the whole branch were then calculated according to the contributions of the different age classes to the total needle area measured on our branches. If differences between $^{13}\Delta$ predicted from gas exchange and $^{13}\Delta_{obs}$ determined from flask measurements were attributed to differences between $C_{i,g}$ and $C_{i,A}$ via stomatal heterogeneity, we would expect similar offsets between conductance-weighted $^{13}\Delta$ and flask $^{13}\Delta_{obs}$ values as between conductance-weighted and assimilation-weighted $^{13}\Delta$ values. But calculated offsets had opposite signs indicating that the differences between predicted and observed $^{13}\Delta$ are unlikely to result from foliage heterogeneity. Moreover, the shift expected from weighting was small (0.24‰) compared to the actual difference between predicted and observed $^{13}\Delta$ values (1.1‰). Although estimating such shifts is limited by the fact that diverse (and even contrasting) patterns of changes in A and g_s across needle age classes have been observed in different studies (Ludlow & Jarvis 1971; Wang 1988), none of these patterns would seem sufficient to induce shifts of the observed direction and magnitude. Again, the more likely explanation is the contribution of further isotopic effects during net uptake such as day respiration, photorespiration and internal CO_2 transfer (see text).